M.Tech (Power System) CHILAKALAPALLI JEEVAN K 2021

MPPT CONTROLLER FOR GRID CONNECTED PV SYSTEM UNDER MISMATCHED ENVIRONMENTAL CONDITIONS

A DISSERTATION SUBMITTED IN PARTIAL FULFILLMENT OF THE REQUIREMENTS FOR THE AWARD OF THE DEGREE OF

MASTER OF TECHNOLOGY
IN
POWER SYSTEM

Submitted By:

Chilakalapalli Jeevan k

(2K19/PSY/06)

Under the Supervision of

Prof. Rachana Garg

DEPARTMENT OF ELECTRICAL ENGINEERING

DELHI TECHNOLOGICAL UNIVERSITY

(Formerly Delhi College of Engineering)

Bawana Road, Delhi-110042

2021

DEPARTMENT OF ELECTRICAL ENGINEERING
DELHI TECHNOLOGICAL UNIVERSITY
(Formerly Delhi College of Engineering)
Bawana Road, Delhi-110042

Declaration

I hereby declare that the work presented in this report entitled "MPPT controller for grid connected PV system under mismatched environmental conditions.", in fulfilment of the requirement for the award of the MASTER OF TECHNOLOGY degree in Power System submitted in Electrical Engineering Department at DELHI TECHNOLOGICAL UNIVERSITY, New Delhi, is a genuine record of my own work carried out under the guidance of Prof. Rachana Garg during my degree.

The work reported in this has not been submitted by me for the award of any other degree or diploma.

Date: 27-10-2021

Place: Delhi

Chilakalapalli Jeevan k (2K19/PSY/06)

DEPARTMENT OF ELECTRICAL ENGINEERING
DELHI TECHNOLOGICAL UNIVERSITY
(Formerly Delhi College of Engineering)
Bawana Road, Delhi-110042

Certificate

This is to certify that Chilakalapalli Jeevan K (2K19/PSY/06) has completed the project titled "MPPT controller for grid connected PV system under mismatched environmental conditions" under my supervision in partial fulfilment of the MASTER OF TECHNOLOGY degree in Power System at DELHI TECHNOLOGICAL UNIVERSITY. I further certify that the publication and indexing information given by the student is correct.

Prof. Rachana Garg
(Supervisor)
(Professor, DTU)

Place: Delhi

Date: 28/10/2021

Acknowledgement

I am very thankful to **Prof. Rachana Garg** (Professor, Department of Electrical Engineering) and all the faculty members of the Department of Electrical Engineering at DTU. They all provided me with immense support and guidance for the project. Without their invaluable time and advice, I would not have been able to conclude my project. I admire her readiness ingenuity to address all my doubts and queries concerning my project. I am thankful to Prof. Uma Nangia, Head of Department, Electrical Engineering Department faculties in Electrical Department, DTU for their kind help, encouragement, and knowledge throughout this course which helped me in completion of my project. I am also grateful to my colleagues and senior research scholars of Electrical Engineering Departments of DTU for helping me in all possible ways to complete my project. I would also like to express my gratitude to the University for providing the laboratories, testing facilities, infrastructure, and environment which allowed us to work without any obstructions.

Chilakalapalli Jeevan K
Roll No. 2K19/PSY/06
Date: 27-10-2021

CONTENTS

List of Figures		
Fig. No.	**Name of the Figure**	**Page No.**
Fig. 1.1	Worldwide electricity generation based on energy resources consumed	4
Fig. 1.2	Categorization of renewable energy sources	6
Fig. 1.3	Grid Connected large Photovoltaic systems	7
Fig. 1.4	Distribution of Renewable Energy in MW as on 31.03.2021	8
Fig. 1.5	India's total installed solar power capacity in megawatts (MW) (till March 2021)	9
Fig. 1.6	Dual stage Grid Connected PV system	10
Fig. 3.1	Ideal Single Diode Model (ISDM)	22
Fig. 3.2	Regular Single Diode Model (RSDM)	22
Fig. 3.3	Simplified Single Diode Model (SSDM)	22
Fig. 3.4	Double Diode Model (DDM)	23
Fig. 3.5	Current-Voltage and Power-Voltage characteristics	25
Fig. 3.6	Buck-boost converter circuit analysis	26
Fig. 3.7	Buck-boost converter waveforms	29
Fig. 3.8	Classification of Single Phase Transformer-less Inverter Topologies	31
Fig. 3.9	Full-bridge converter	32
Fig. 3.10	An RL load has a square wave output voltage and a steady-state current waveform	35
Fig. 3.11	Unipolar SPWM waveform	37
Fig. 3.12	Inverter output voltage with Unipolar SPWM	38
Fig. 3.13	Bipolar SPWM waveform	38
Fig. 3.14	Inverter output voltage with Bipolar SPWM	39
Fig. 3.15	Dual Buck & Boost based Inverter (DBBI)	40
Fig. 3.16	Buck stage and Boost stage of the proposed inverter	40
Fig. 3.17	Control logic of the proposed system	42
Fig. 4.1	Fixed Voltage Maximum power point technique for Solar PV system	46
Fig. 4.2	Current-voltage, Power -voltage characteristics of the typical PV panel	48
Fig. 4.3	Perturb and Observe Maximum power point technique for Solar PV system	49
Fig. 4.4	Power-Voltage characteristics of typical PV Panel	50
Fig. 4.5	Flow Chart for PO MPPT	51
Fig. 4.6	Incremental Conductance Maximum power point technique for Solar PV system	53
Fig. 4.7	Power-Voltage characteristics of typical PV Panel	53
Fig. 4.8	Flow Chart for Incremental Conductance MPPT	55
Fig. 4.9	Membership function for Error	57
Fig. 4.10	Membership function for rate of change of Error	58
Fig. 5.1	The overall Simulink model of the solar PV integrated with grid system	61
Fig. 5.2	The control algorithm for the proposed system	62
Fig. 5.3	Simulink model of incremental conductance MPPT	62

List of Tables		
Table. No.	**Name of the Table**	**Page No.**

List Of Symbols and Abbreviations	
Symbols and Abbreviations	**Description**
AC	Alternating Current
C	Capacitor
DC	Direct Current
EMC	Electromagnetic Compatibility
EMI	Electromagnetic Interference
IC	Integrated Chips
IEEE	Institute of Electrical and Electronics Engineers
IGBT	Insulated Gate Bipolar Transistor
I_{rms}	RMS current
KV	Kilo Volt
L	Inductor
MLI	Multilevel Inverter
MOSFET	Metal Oxide Semiconductor Field Effect Transistor
MPPT	Maximum Power Point Tracking
MW	Mega Watt
NPC	Neutral Point Clamped
P_{IN}	Input power
P_{LOSS}	Power loss
P_{OUT}	Output power
PV	Photo Voltaic
PWM	Pulse Width Modulation
R_L	Resistor
RMS	Root Mean Square
THD	Total Harmonic Distortion
V_{dc}	DC voltage
$V_{O,MAX}$	Maximum output voltage
V_{peak}	Peak voltage
V_{rms}	RMS voltage
VSI	Voltage Source Inverter
η	Efficiency

ABSTRACT

The demand for electrical energy is increasing exponentially and conventionally fossil fuels are greatly used to meet that demand. With growing concern about environment, to meet this increased demand, application of Renewable Energy Sources (RES) has been in light. Solar PV has garnered greater attention for power generation among various RES such as wind energy, fuel cells, biogas, and photovoltaic (PV) systems due to its large availability, low maintenance, and pollution-free nature. Solar cells/modules convert solar energy directly into electrical energy. The characteristics of PV depend upon irradiation and temperature. The temperature and the irradiation of the solar cell depend on the atmospheric conditions. As a result, tracking the maximum power point (MPP) in any scenario is vital to achieve that the PV panel produces the maximum possible power.

The major goal of this study is to come up with the optimum Maximum Power Point Tracking (MPPT) algorithm for controlling a grid-connected solar PV system under varying environmental conditions. In this work a 700W grid connected solar PV system consisting solar PV array, buck-boost converter, inverter, MPPT controller and inverter control is designed. The modelling and simulation are done in MATLAB/Simulink software. For the proposed system conventional MPPT algorithm- incremental conductance is developed and implemented. The conventional MPPT algorithm- IC have slower speed and high cost; in order to increase the efficiency of tracking intelligent controller is included in the MPPT technique. A fuzzy based maximum power point tracking algorithm is proposed for grid connected solar PV system under mismatched environmental conditions. The fuzzy based maximum power point tracking algorithm is based on a sugeno type fuzzy logic controller with uncertainty handling capabilities. Changes in PV voltage and power are regarded inputs to the fuzzy based controller, while a change in duty cycle is considered the output of the fuzzy based controller.

In order to validate the effectiveness of the developed MPPT control, two set of working conditions for analysis such as steady state irradiance and step dynamic change irradiance are considered in MATLAB / Simulink environment. The developed controller is compared with each other in terms of maximum power ratio, transient time, and overshoot.

CHAPTER 1

Introduction

1.1. General

Electricity is the most useful and efficient kind of energy amongst several other forms of available energies owing to its multiple advantages such as transmissibility, controllability, storability, ease of use and cleanliness etc. Traditional energy sources such as coal, crude oil, and natural gas continue to be the dominant sources of electricity generation, although renewable resource use has steadily expanded since the 1970s. The emergence of renewable energy sources has been aided by both global energy demand and technological advancements, as seen in Fig. 1.1. Despite the fact that converter efficiency is improving, global energy market is anticipated to expand until 2040.

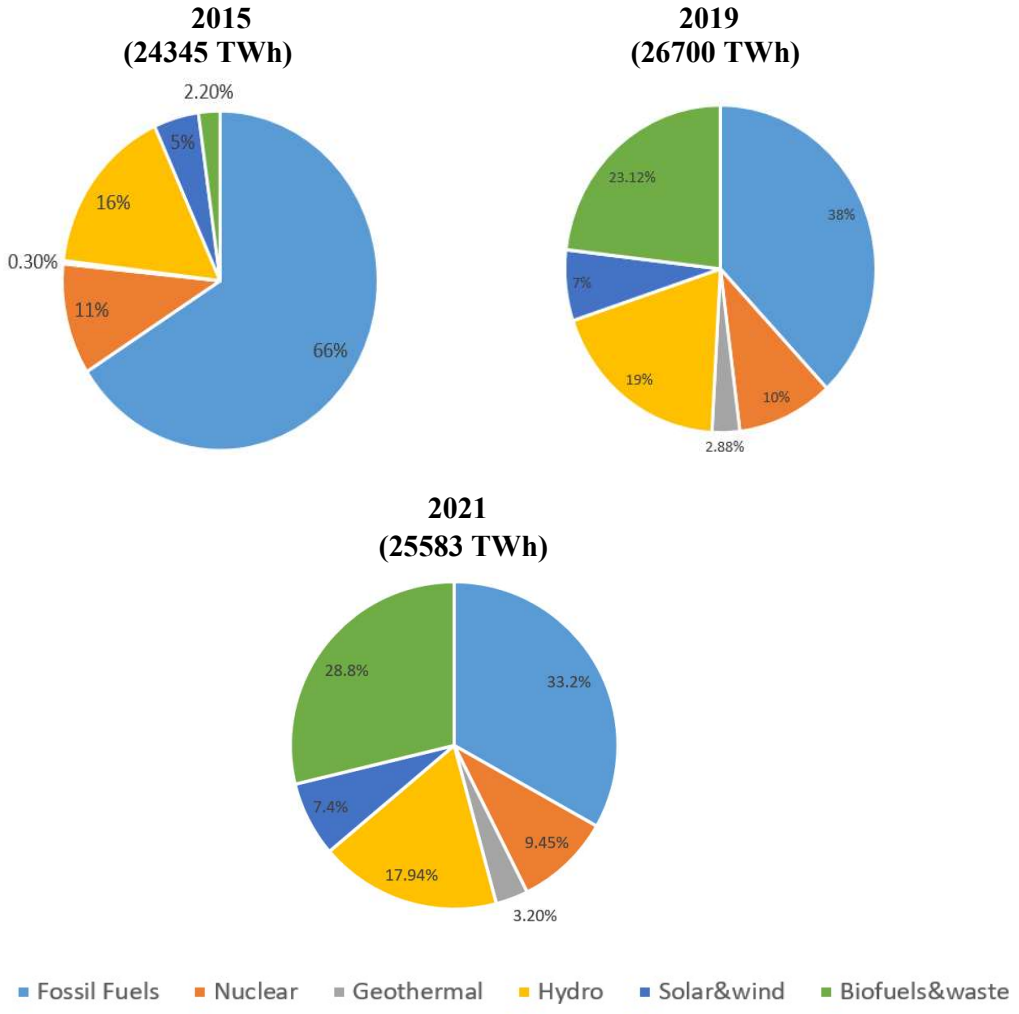

Fig. 1.1: Worldwide electricity generation based on energy resources consumed.

Renewable energy resources are expanding rapidly and are expected to grow at a rate of 2.6 percent per year globally until 2040. The integration of utilities and renewable energy sources benefits both the economy and the environment. The main challenge for an integrated system, however, is to compensate for varying energy supply due to changing atmospheric conditions and to sustain economic competitiveness with conventional sources. Clean energy resources have also piqued the interest of countries seeking to reduce their carbon footprints.

Renewable energy sources are portion of India's perception, which includes not only bringing clean and affordable energy to all people, but also achieving social equity and addressing ecological challenges. Using these energy sources has helped India achieve a cleaner environment, energy independence, and a more stable monetary system. India has ascertained that the finest approaches for expediting deployment, stimulating innovative businesses, and meeting climate change mitigation goals are implemented.

India is well on its path to achieving its target, with over 96.96 GW of installed renewable power capacity and 78 GW in various phases of development. Solar power capacity has increased by more than 11 times since 2014, while wind power capacity has increased by 1.7 times. India now has the world's fourth largest deployed renewable energy capacity. This, however, is only the early stages and by no means a limit on the aspiration.

Fostering an environment conducive to indigenously developing renewable energy technologies and aiding domestic manufacturing, dealing with renewable power intermittency, enhancing forecasting technology, developing a productive and adaptable renewable power transmission infrastructure, and constructing storage technologies are the challenges, and we have been attempting to make concerted efforts in this direction. Strategic research into renewables focuses on improving technology performance and affordability; next generation photovoltaic and energy storage technologies are high on the priority list. Coordination of research is being carried out by R&D institutions, industry, and universities. We are analysing both domestic and international efforts in these sectors.

According to the National Electricity Plan 2020, renewable power capacity will reach 275 GW by 2027. Numerous different analysis suggests that by 2030, an electric installed capacity of 860 GW would be required, with solar and wind power making a contribution approximately 500 GW. These will necessarily entail a major departure from business as

usual, requiring a new paradigm with support mechanisms, easier policies, and encouraging innovation and capital. The incorporation of renewables into India's energy supply is member of the country's 2030 vision, and it is also dedicated to the global goal of achieving sustainable development and dealing with climate change.

1.2. Renewable Energy

Conventional energy sources and nuclear energy cannot meet the world's energy demand indefinitely. This is because the replenishment rate of these sources is very sluggish, and thus they cannot be used indeterminately. Furthermore, when used to generate electricity, they pollute the environment. An improved solution to the problems listed above is to use renewable energy resources, which are environmentally friendly, economically viable, and provide socioeconomic benefits by creating jobs. All of this is consistent with the concept of sustainable development's three pillars (i.e. economic, environmental and social sustainability).

Renewable energy resources are renewed on a continuous basis by the sun or other natural phenomena. The sun is used directly in the production of thermal, photochemical, and photoelectric energy. whereas biomass, wind, and hydro use the sun's energy indirectly. Geothermal and tidal energy are produced by the earth's crust and the moon's gravitational pull, respectively. The multiple kinds of renewable energy resources have been categorised in Fig.1.2.

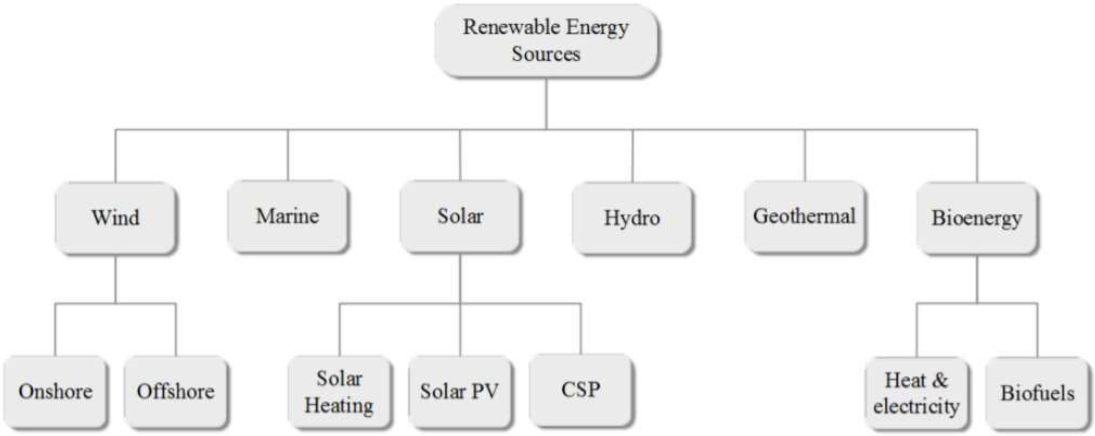

Fig.1.2: Categorization of renewable energy sources.

Over the course of more than a century, conventional energy resource technologies have grown and developed. Vast sums of money have been invested in research and

development. In recent times, a substantial investment is necessary to accomplish marginal improvement, whereas renewable energy resources are in a development phase where a small investment in R&D results in significant system efficiencies and commercial feasibility.

Power electronics is an engineering branch of that has made significant contributions to the advancement of this technology. A DC-AC power electronic converter (inverter) is used to retrieve as much energy as possible from a PV system and distribute it to the power grid or other AC loads. The converter's job in wind systems is to increase energy extraction while also regulating changing input wind power. All of this is facilitated by an understanding of power electronics as well as a control system. Figure 1.3 depicts a common grid-connected topology for a solar energy system.

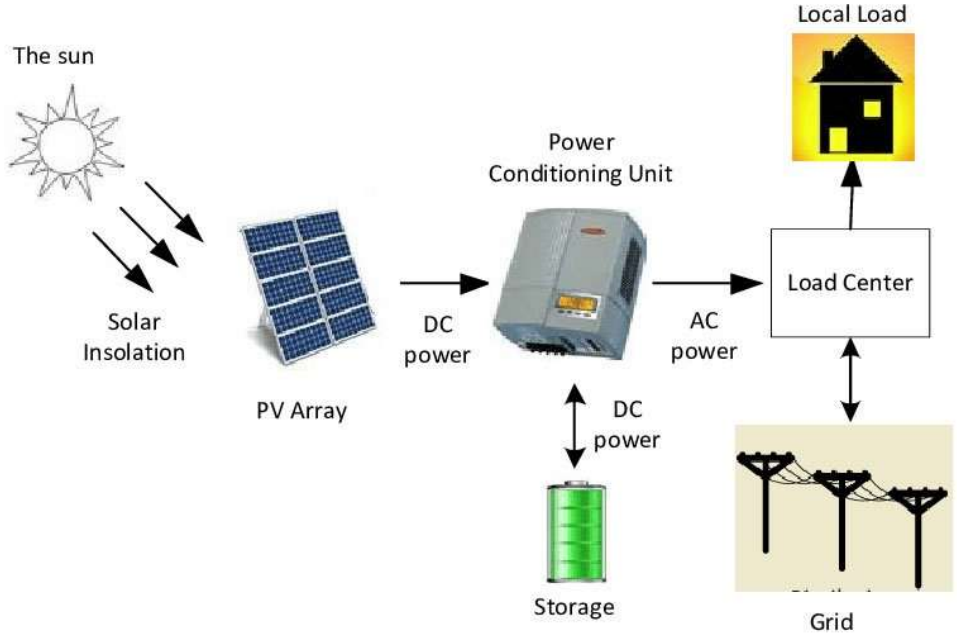

Fig. 1.3: Grid Connected large Photovoltaic systems.

India is leading the world in terms of renewable energy capacity expansion. India declared its ambition to double its renewable energy target from 175 GW to 450 GW by 2022 at the United Nations Climate Summit in 2019. By that time, modern renewable energy sources such as geothermal and tidal are expected to increase dramatically. This goal includes doubling wind power capacity and boosting installed solar energy capacity by 15 times above what it was in April 2016. With such lofty goals, India will be capable of leading the world in the usage of renewable energy sources and will play a significant

role in the International Solar Alliance's "sunshine countries" initiative. This project encourages the growth and development of solar energy sources for the 120 countries that lie inside the Earth's equatorial belt, which obtains sunlight for the majority of the year.

It is evident that energy is critical to any country's development. India is the world's second-largest population after China, accounting for roughly 18% of the total global population. India ranks fourth in the world in terms of energy consumption due to its growing population and rising level of living. Because the usage of decreasing fossil fuels has resulted in significant pollution, leading to global warming and climate change, renewable energy is the best option. This is because energy demand is increasing every day, and proper use of both resources is the solution for today's problems.

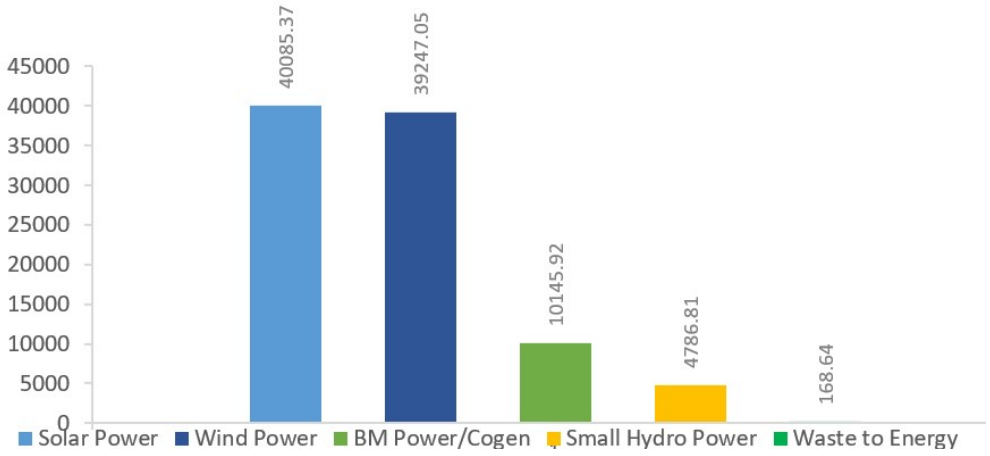

Fig. 1.4: Distribution of Renewable Energy in MW as on 31.03.2021.

Since many countries lack access to a solar electrical grid, solar energy was first used in agriculture, water pumping, and lighting. Some huge solar projects have indeed been considered, such as one in the Thar dessert (which covers 35,000 km2), which is expected to generate 700-2100 GW of power. Solar power in India is growing at a rate of roughly 113 percent per year, and the energy cost has plummeted to Rs. 4.34 per kWh. This figure is 18 percent less than the average cost of coal-fired electricity.

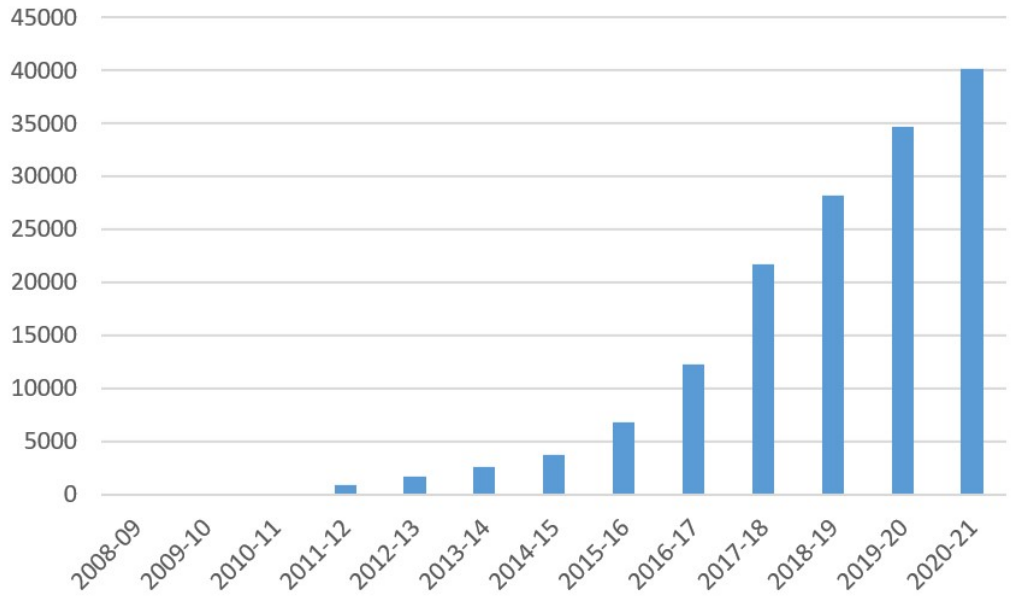

Fig. 1.5: India's total installed solar power capacity in megawatts (MW) (till March 2021).

Renewable energy will surpass fossil fuels as the primary source of energy by 2040, as per British Petroleum's Annual Energy Outlook 2019. According to the IEA's Annual Energy Outlook 2020, affordable renewable technology, digitalization, and the rising importance of electricity are key drivers of development. According to the report, the globe is experiencing a huge shift in energy consumption, with India's need expanding at the fastest rate.

1.3. Research Objectives

Most important thing in the solar PV array is maximum power extraction. Solar PV panel has nonlinear power output due to non-uniform environmental or climate condition and power semiconductor materials used in the PV panel. In general, the Fixed Voltage method, Perturb and Observe method (PO), and Incremental Conductance method (INC) are used to extract the maximum power from a solar PV system. However, such methods have some drawbacks, such as the Fixed Voltage method's inability to extract maximum power when the PV panel's cell temperature varies, and the PO & INC methods extract maximum power from the PV system but oscillate around the maximum power point.

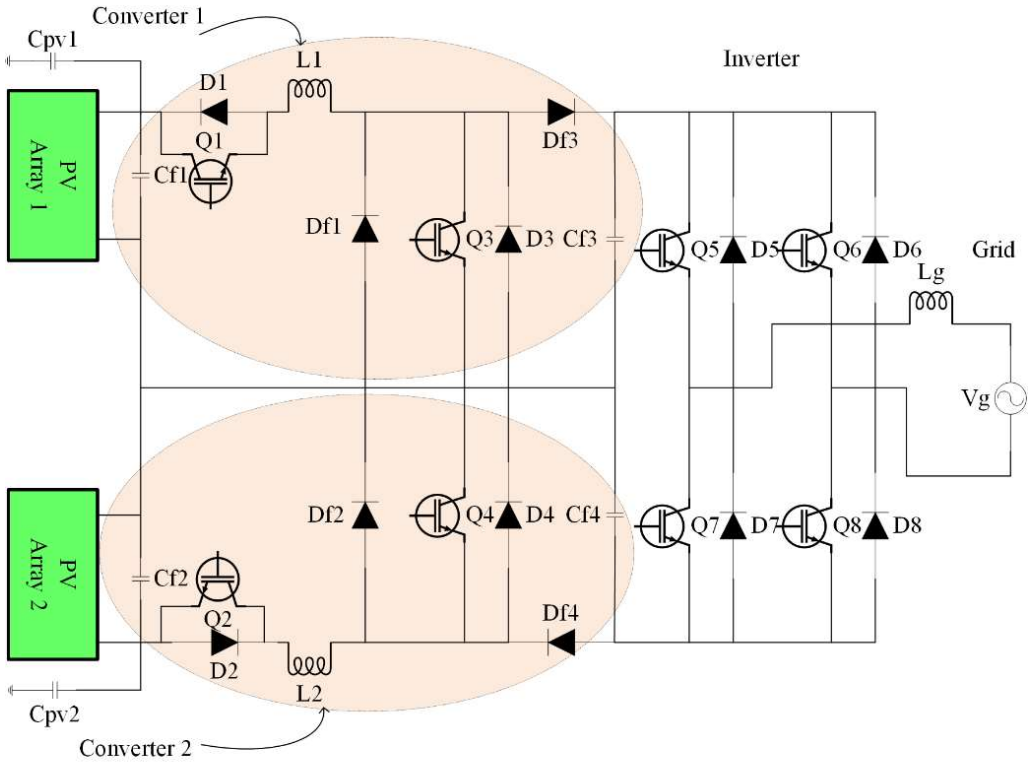

Fig. 1.6: Dual stage Grid Connected PV system.

In general, there are two ways to connect a solar PV array to the grid: Single stage connection and Double stage connection. In single stage connection, solar PV array is directly connected to the grid via inverter with some grid control logic and this method of connection only useful when terminal voltage of the solar PV array within specified level. if terminal voltage of the solar PV array is low then double stage connection is preferred. Between the solar PV array and the grid inverter, a dual buck boost dc-dc converter is employed to regulate the power flow and terminal voltage re-equipment.

Organization of the Thesis

The following chapters are presented in this thesis as follow:

1. In chapter 1, Need of Renewable Energy in day to day life, its categorization, statistics in India in RE sector, and research objective have been discussed.

2. In chapter 2, the literature evaluation of the study given in the thesis is presented.

3. In chapter 3, modelling and design of grid connected PV system is discussed.

4. In chapter 4, Working principle of the Proposed system and its Control circuit has been discussed.

5. In chapter 5, Fuzzy MPPT for solar PV fed dual buck-boost converter based single phase gird integrated PV system is presented. Simulation results of the incremental conductance MPPT and fuzzy MPPT for solar PV fed dual buck-boost converter based single phase gird integrated PV system are compared.

6. In chapter 6, Conclusion and Future scope is discussed.

.

CHAPTER 2

Literature Survey

2.1. General

This chapter is an overview of some of the works done previously on MPPT control of PV system. Following topics are covered here as mentioned below:

i. Solar PV system
ii. MPPT techniques
iii. Inverter control techniques

2.2. Literature review on Maximum Power Point Tracking Algorithm

The extraction of maximum power is still challenging in various atmospheric conditions and change in irradiation. In addition, power generation of the PV panels are low in partial shaded condition. Abdouramani Dadjé et al. (2016) have presented the various approach of MPPT algorithm for extracting maximum power under partial shaded conditions. The novel approach perform well compare to other conventional techniques under various conditions [11].

Rozana Alik et al. (2017) has proposed a modified P& O algorithm with variable step size and high tracking speed. The proposed technique is analyzed in two different cases such as constant irradiation and variable irradiance and it achieves high speed convergence, low output ripples and good accuracy. However, the implementation of this method is complex and expensive [45].

P&O MPPT algorithm is presented for low voltage rated DC/ DC converter by Jirada Gosumbonggot et al. (2016). The switching of converter is improved with opto coupler-based gate driver circuit. The voltage and current signal are observed with proper controller circuit and achieve better voltage regulation with low voltage distortion. However, the addition of sensors raises the cost of the circuit and increases the controller's complexity. [26].

Another MPPT technique is incremental conduction algorithm, which is most frequently used in PV system and have special feature like low switching frequency and

high accuracy than the P& O MPPT as presented by Ratna Ika Putri (2014). However, because the duty cycle is modified over a large range in order to maintain the ideal spot, tracking time is slow and power loss is high. [42].

Lipschitz Optimization is a novel MPPT technique for PV systems operating in partial shading conditions. It tracks the highest point from the voltage-power curve because several peak points are formed in this situation. Wenfan Li (2019) compared the performance of the presented technique with modified Particle Swarm Optimization and Firefly Optimization algorithms, achieve fast tracking speed and high efficiency than the compared methods [31].

Tsung-Wei Hsu (2019) has developed a (Internet of Things) IoT tracking technique with fractional open-circuit voltage method for low power generation. The pulse-frequency modulation is employed for gate pulse generation for converter switches; however, the ratio of the open circuit voltage and maximum voltage is varied for each panel and create a charge balancing problem in the capacitor [24].

Particle Swarm Optimization MPPT is developed for PV application to improve the speed of tracking and conversion efficiency by eliminating the random and inferred variables. In order to compute the inertia factors and random variables, functional analysis is used and obtained better result than the conventional particle swarm optimization method as reported by Keyong Hu (2019). However, the implementation of the presented technique is complex and expensive [25].

Hegazy Rezk et al. (2019) have proposed an suggested fuzzy logic based MPPT for PV system with fast convergence, tracking speed, high accuracy and simple algorithm. This method overcomes the shortcoming of the standard fuzzy logic MPPT method at slow and fast variation in the irradiance and climatic changes. Even though, the presented technique obtains maximum power with low ripple, the Framing the membership function for the symmetric and asymmetric type is quite difficult in dynamic condition [43].

A hybrid model of MPPT method is presented for three phase grid connected application with anti-islanding protection by Padmanaban et al. (2019). The presented technique includes the feature of the ANFIS and Artificial B Colony techniques, it yields the results of minimized root mean square error and obtain the optimum membership function. Fuzzy algorithm is incorporated for generating the gate pulse for the three-phase inverter to convert the SEPIC converter output and inject the pure sinusoidal signal to the

grid system, hence the manipulation and implementation is complex for real time application [37].

Khaled Bataineh (2019) employs another hybrid technique for PV application with combination of fuzzy logic with incremental conduction and fuzzy logic with P& O algorithm. The proposed approaches are evaluated for a variety of irradiation situations, including uniform irradiation, abrupt variations, and partial shading, and they improve the system's performance rather than operating as independent MPPTs. [29].

Mhamed Fannakh et al. (2016) have implemented a hardware model for arduino based real time PV system with intelligent controller. The fuzzy logic is employed as tracking tool for maximum power harvesting to enable the boost converter with duty cycle calculation. However, the PWM technique is high switching frequency modulation technique that enhances the converter's switching frequency while lowering the system's efficiency. [34].

Caio Meira Amaral da Luz (2020) has analyzed varies MPPT techniques under the uniform and variable irradiance state, and found that traditional algorithms are insufficient for determining the global maximum power point when partial shaded panels are used. Even though, the golden section optimization has achieved good accuracy, high tracking speed and conversion efficiency than the conventional techniques, the implementation is difficult for large-size PV panels under partial shading condition [18].

Partial shading condition is a common problem in the PV panel, which create the hotspot in the panel and produce multiple peaks in the output voltage waveform. To boost the panel output, the authors Yingquan Zou et al. (2019) employed differential flatness control theory to linearize the output voltage values and then a fuzzy logic based MPPT method to monitor the maximum power point. [52].

The most appropriate methodology for power point tracking the PV system is fuzzy based MPPT, however it is difficult to improve the speed of the tracking process. A hybrid technique is introduced with combination of three-point tracking algorithm with fuzzy logic controller which considerably decreases the power loss and increase the efficiency of the PV arrays. However, the presented technique requires high convergence period to manipulate the membership functions [13].

The static and dynamic partial shading is another challenge in the roof top plants, in this scenario, irradiation forecasting data is used to enhance the highest power point. Rajneesh Kumar (2019) have analyzed the dynamic state of the converter with modified incremental conduction method; however, the memory requirement is high for implementing in the real time operation [14].

Loghman Samani & Rahmatollah Mirzaei (2019) have developed predictive control model whereas the voltage and current is analytically determined using system model and the maximum power point is obtained with the cost function. Further, fuzzy based tracking is employed to achieve the steady state and dynamic response quickly even the rapid changes in the insolation [49].

Mostafa R Mostafa et al. (2018) have designed a sliding mode controller to eliminate the oscillation during the selection of maximum power point in P& O MPPT algorithms. The steady state response is obtained within the limit by setting the operating point and the gate pulse is controlled to operate the DC/ DC converter, then the output is fed to seven level multilevel inverter. Even though, the output has stabilized and faster than the P& O technique, the voltage stress on switches is high for high voltage application [35].

Danandeh et al. (2018) has introduced a hybrid control with the advantage of fuzzy system and incremental cost algorithm which locate the global peak at partial shading and other atmospheric condition. In this, the presented hybrid techniques achieves high accuracy, low cost, simple implementation, and reduced number of fuzzy rules and then increases the efficiency of the converter with low switching frequency operation. The increase of temperature in PV panels and nonlinear variation of insolation causes to reduce output of the system [19].

Nurul Afiqah Zainal (2016) has designed a cooling system to maintain the optimum temperature of the panels and the fuzzy based constant voltage MPPT algorithm is employed to increase the maximum power tracking. The cost of the cooling system, however, is limited by the use of a high number of PV panels. [51].

The conversion capabilities of the PV arrays, the switching of the DC/DC converter, and the output of the three-phase inverter all contribute to the grid linked PV system's efficiency. The maximum power is obtained from the ANN based MPPT algorithm as presented by Houria Boumaaraf et al. (2015). In order to improve the inverter

output, three phase multilevel inverter is used and produced better output compared to two level inverters, since NPC inverter have ground terminal in the middle point which stabilize the output of the PV panels [23].

Saban Ozdemir et al. (2017) have designed and developed adaptive fuzzy based perturb and observe maximum power point tracking (MPPT) for solar PV system. The designed MPPT algorithm incorporates the merits of both Fuzzy logic and Perturbs and Observe algorithm. Using the current and voltage of the solar PV system, the adaptive Fuzzy MPPT determines the duty ratio of the boost converter. This method outperforms the standard Perturb and Observe method in terms of steady state response and maximum power conversion ratio. [46].

Rather than using traditional MPPT techniques, intelligent controllers play a significant role in PV applications for maximum power tracking under diverse insolation and partial shading situations. The authors Faiza Belhachat (2017) have proposed ANFIS technique to extract maximum power in typical operating condition. To regulate the output power from the input voltage and current data, the ANFIS employs the least squares estimator and the gradient approach. The presented technique, on the other hand, maximizes the peak power value; however, there is a little fluctuation in the output for the number of PVs connected in series. [20].

The Incremental conductance maximum power point tracking algorithm for solar PV electrical systems was developed by RatnaIka Putri et al. (2015). The incremental conductance is compared to the instantaneous conductance in this method to increase or decrease the reference voltage. How quickly the maximum power point is tracked is determined by the increment step size. With large step increments, quick tracking can be achieved; however, the approach may not operate precisely at the maximum power point and oscillate about it. [42].

Ammasai Gounden et al. (2009) created a fuzzy maximum power point tracking method for a grid-connected solar PV electrical system, demonstrating that the fuzzy logic MPPT is a useful tool for extracting maximum power from solar PV systems. To deal with real-time applications, fuzzy logic control uses human expert knowledge rather than mathematical transfer functions. The fundamental drawback of the fuzzy logic-based approach is that as the number of parameters in the membership function and the fuzzy

rule base grows, so does the number of parameters in the membership function and the fuzzy rule base. [6].

Khanaki, Razieh et al. (2014) used artificial neural networks to design a maximum power point algorithm for solar PV electrical systems. With abrupt changes in the ambient conditions, the MPPT algorithm based on artificial neural networks can extract the maximum power precisely and quickly. The artificial neural network MPPT approach, on the other hand, has significant drawbacks, such as the need to train the neural network model on a regular basis to ensure convergence to the exact maximum power point. In general, artificial neural network MPPT algorithms have superior performance under different operating conditions; although, ANN MPPT algorithms are complex to apply on the marketable PV system, since several variables which decide the performance of the algorithm require to be set by the engineer [28].

2.3 Conclusion

The literature review for the work done in "Design and modelling of Maximum power point tracking (MPPT) approaches for solar PV systems" is contained in this chapter. A literature review of grid connected PV systems and MPPT control is conducted in order to have a better understanding of PV systems.

CHAPTER 3

Design of Solar PV System

3.1. General

Solar PV systems capture energy in the form of electricity, which is then used to fulfill load demand. Because solar PV systems rely on sunlight to generate electricity, environmental conditions such as temperature and irradiance have a significant impact on their output. To accommodate for this unpredictability, the SPV system is either connected to the grid or uses a battery as an energy storage element. As a result, solar PV systems are grouped into two types: stand-alone PV systems and PV systems that are connected to the grid. PV arrays, power conditioning elements, and interconnected loads are the basic components of a solar power generation system. Solar PV arrays are powered by solar modules in different configurations, each of which contains solar cells. Power electronics equipment such as DC-DC converters and inverters (dc to ac) are used as power conditioning devices between the PV array and the load. This chapter explains how to design a solar PV system.

3.2. Photovoltaic System

One or more solar panels, an inverter, and other electrical and mechanical components make up a photovoltaic (PV) system, which uses the Sun's energy to generate electricity. PV systems are available in a variety of dimensions, ranging from simple rooftop or compact units to massive utility-scale power plants.

3.2.1. Photovoltaic Effect

The PV effect is the process of converting sunlight into direct power. A junction is formed when two semiconductors, usually silicon, are joined together. This newly formed confluence is known as the p-n junction. There are two kinds of semiconductors in the p-n junction: n-type and p-type semiconductors. Doping trivalent impurity forms the n-type semiconductor, and likewise, doping pentavalent impurity forms the p-type semiconductor.

Excess electrons are moved from n-type to p-type semiconductors through the junction, whereas excess holes are transferred from p-type to n-type semiconductors. An electric field is created at the junction when n-type and p-type regions are formed. Electron-hole

pairs are formed when photons from the sun with an energy greater than the material's band gap energy fall on the PV cell. The electrons begin to traverse the circuit due to the electric field present at the cell's junction. After completing the circuit, the electrons reunite with the holes. The direct current is created by the movement of electrons.

3.2.2. Types of Photovoltaic Cells

Monocrystalline and Multi crystalline PV cells are the two types of PV cells utilised in conventional PV panels. Mono-crystalline provides the benefit of improved efficiency but has the disadvantage of higher manufacturing costs. Multi-crystalline cells, on the other hand, are of lesser quality because they feature gain borders, which diminish cell efficiency by introducing boundary losses.

3.2.3. Solar Spectrum

The solar irradiation that strikes the atmosphere differs from that which strikes the land. Geographical position, weather, pollution levels, climatic fluctuations, and variations in the day all contribute to changes in irradiation. To aid standardise measurements, the American Society for Testing and Materials has established a defined coefficient for air mass.

The coefficient is calculated by dividing the real sunlight route length from the atmosphere to the surface by the virtual normalised zenith path length. As a result, the coefficient is 1 when the sun is directly overhead, and AM1 can be utilised. In the medium or temperate latitudes, the AM1.5 coefficient is employed. AM1.5 is the standard testing setting, with a 1 KW/m2 irradiation and a room temperature of 25° C.

3.2.4. Photovoltaic Cell Models

The single diode model (SDM) and the double diode model (DDM) are two methods for computing the equivalent circuit of a PV cell (DDM). The number of distinct diodes employed in the model circuit divides these models. The parasitic power losses are shown by modelling the resistances for the shunt and series parts.

3.2.4.1. The Single Diode Model (SDM)

The different components of SDMs are the ideal single diode model (ISDM), the regular single diode model (RSDM), and the simplified single diode model (SSDM) (SSDM). The ISDM is the simplest, with only three parameters. The fundamental disadvantage of

ISDM, however, is that it does not guarantee good simulation results. Because of the inclusion of series and shunt resistances, the RSDM provides better accuracy than the ISDM, but it necessitates solving for five equations. The SSDM ignores shunt resistance to simplify modelling, however it produces erroneous results with changing insolation and temperatures.

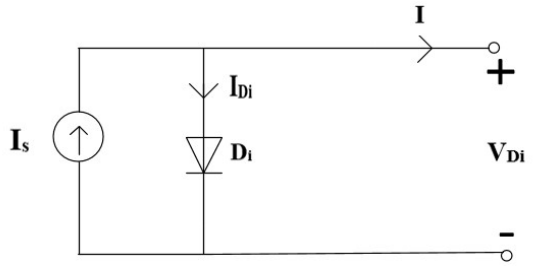

Fig. 3.1: Ideal Single Diode Model (ISDM)

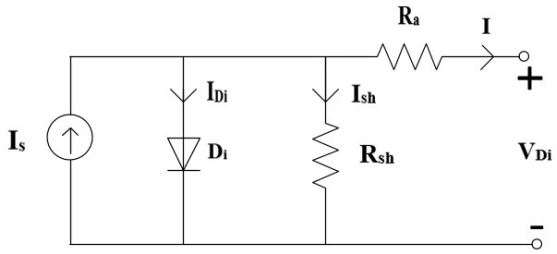

Fig. 3.2: Regular Single Diode Model (RSDM)

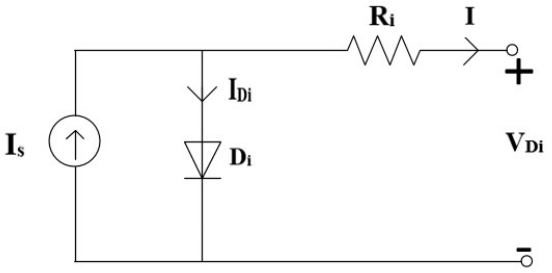

Fig. 3.3: Simplified Single Diode Model (SSDM)

The following equations are developed using the Regular Single Diode Model (RSDM).

Using Kirchhoff's Law:

$$I = I_S - I_{Di} - I_{sh} \tag{3.1}$$

Where I_{Di} is diode current, I_{sh} is shunt current and I is total output current.

Using Kirchhoff's Law:

$$V_{Di} = V + I * R_i \tag{3.2}$$

Here, the output voltage is V, the shunt resistance is Ri, and the diode voltage is VDi.

Using Ohm's Law:

$$V_{Di} = I_{sh} * R_{sh} \tag{3.3}$$

Here, resistance means shunt resistance.

Substituting Eq. (3.3) in Eq. (3.2):

$$I_{sh} = \frac{V_{Di}}{R_{sh}} = \frac{V_{Di}+IR_i}{R_{sh}} \tag{3.4}$$

From the Schottky Diode Equation we have:

$$I_{Di} = I_s[e^{\frac{V_{Di}}{nV_T}} - 1] \tag{3.5}$$

The thermal voltage is expressed as:

$$V_T = \frac{k_B * T}{q} \tag{3.6}$$

The cell's temperature is T, the Boltzmann constant is kB, and the electron charge constant is q. We may get the final form of the I-V characteristics equation for a single PV cell using the RSDM by substituting Eqs. (3.4) through (3.6) into Eq. (3.1).

$$I = I_s - I_{sr}\left(e^{\left(\frac{V+IR_i}{nV_T}\right)} - 1\right) - \frac{V_{Di}+IR_i}{R_{sh}} \tag{3.7}$$

3.2.4.2. The Double Diode Model (DDM)

Although the double diode model is more precise than the single diode model, it also has the disadvantage of being more complex. This model does not ignore recombination losses in the depletion zone, hence the results are reliable.

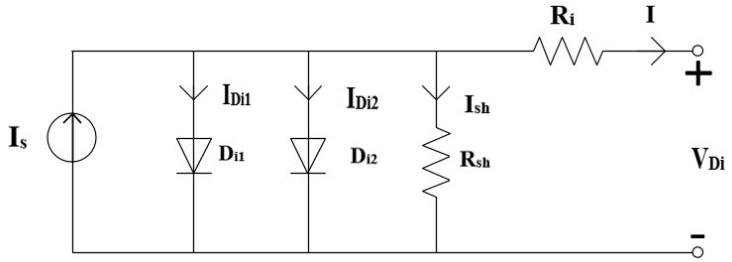

Fig. 3.4: Double Diode Model (DDM)

The current-voltage characteristics is calculated using the equivalent circuit using the equation:

$$I = I_s - I_{Di1} - I_{Di2} - \frac{V+IR_i}{R_{sh}} \quad (3.8)$$

The diode currents are given below:

$$I_{Di1} = I_{s1}[e^{\frac{V_{Di}}{nV_T}} - 1] \quad (3.9)$$

$$I_{Di2} = I_{s2}\left[e^{\frac{V_{Di}}{nV_T}} - 1\right] \quad (3.10)$$

More equations must be developed for the simulation investigations, which are as follows:

With Ns signifying the count of serially connected cells and Np denoting the quantity of parallelly connected cells, the equation for the PV array, w.r.t Eq. (3.7) is:

$$I = N_p I_{ph} - \frac{N_p I_{ph}}{\left[e^{\frac{V_{Di}}{nV_T}} - 1\right]}\left[e^{\frac{\frac{V}{N_s}+\frac{IR_i}{N_p}}{nV_T}} - 1\right] - \frac{\frac{N_p}{N_s}V+IR_i}{R_{sh}} \quad (3.11)$$

Based on the amount of solar energy it absorbs and the device's operating temperature, the photocurrent equation is used to calculate how much photocurrent the PV cell(s) create.

$$I_s = [I_{sci} + K_i(T - 298)]\frac{I_{rri}}{1000} \quad (3.12)$$

The reverse saturation current is given as,

$$I_{rri} = \frac{I_{sci}}{[e^{\left(\frac{V_{oci}}{nN_sV_T}\right)} - 1]} \quad (3.13)$$

$$I_{sr} = I_{rri}\left(\frac{T}{T_r}\right)^3 e^{[qE_q\frac{\left(\frac{1}{T_r}-\frac{1}{T}\right)}{nki}]} \quad (3.14)$$

The following equation can be used to represent the diode current in a PV array, using Ns as the number of series cells and Np as the number of parallel cells:

$$I_{Di} = I_{sr}\left[e^{\frac{\frac{V}{N_s}+\frac{IR_i}{N_p}}{nV_T}} - 1\right] \quad (3.15)$$

3.2.4.3. Output Characteristics of a PV Module

The PV module's I-V and P-V characteristics are shown using the following parameters.

Table 3.1 Specification of Solar PV array

PARAMETER	VALUES
OPEN CIRCUIT VOLTAGE (V)	35.7
SHORT CIRCUIT CURRENT (A)	6.45
VOLTAGE AT MAXIMUM POWER POINT (V)	28.7
CURRENT AT MAXIMUM POWER POINT (A)	5.76
VOLTAGE TEMPERATURE COEFFICIENT	-0.37
CURRENT TEMPERATURE COEFFICIENT	0.08
SERIES NUMBER OF PANEL	4
PARALLEL NUMBER OF PANEL	1
MAXIMUM POWER OF PV ARRAY (W)	700

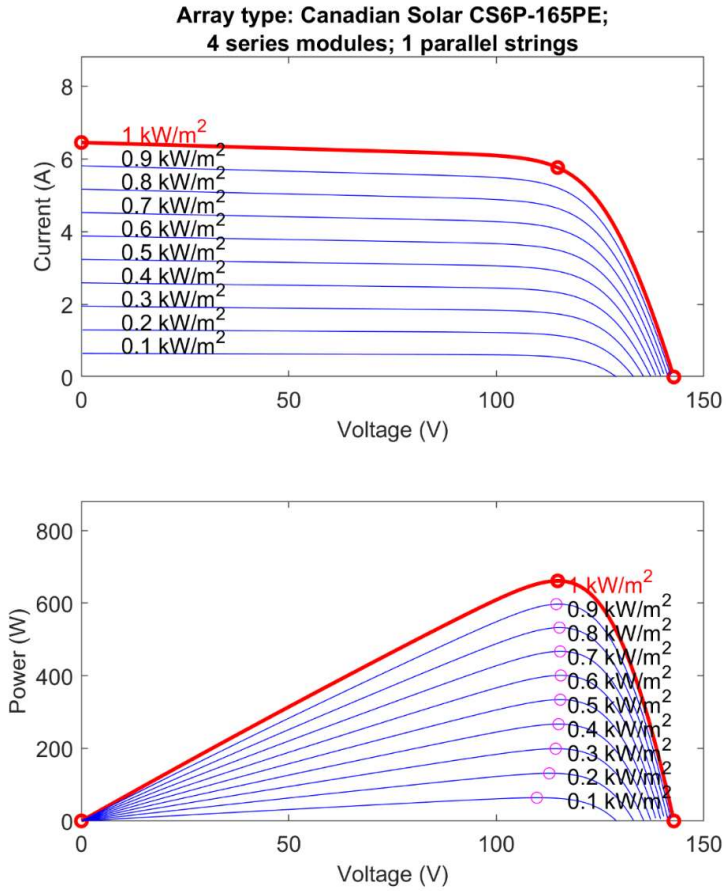

Fig.3.5: Current-Voltage and Power-Voltage characteristics.

3.3. Design of DC-DC Converter

There are three basic types of DC-DC Converters namely: Buck Converter, Boost Converter, Buck-Boost Converter. In this work, we have worked on Buck-Boost Converter.

3.3.1. Basic designing of Buck-Boost Converter

Another fundamental switched-mode converter is the buck-boost converter, as shown in Fig. 3.6. The output voltage of a buck-boost converter might be higher or lower than the input voltage.

Voltage and Current Relationships

The following are some assumptions concerning the operation:

1. The circuit is in a steady state of operation.

2. The current in the inductor is steady.

3. The capacitor is large enough to ensure that the output voltage remains constant.

4. For time DT, the switch is closed, and for (1-D) T, it is open.

5. The components are ideal.

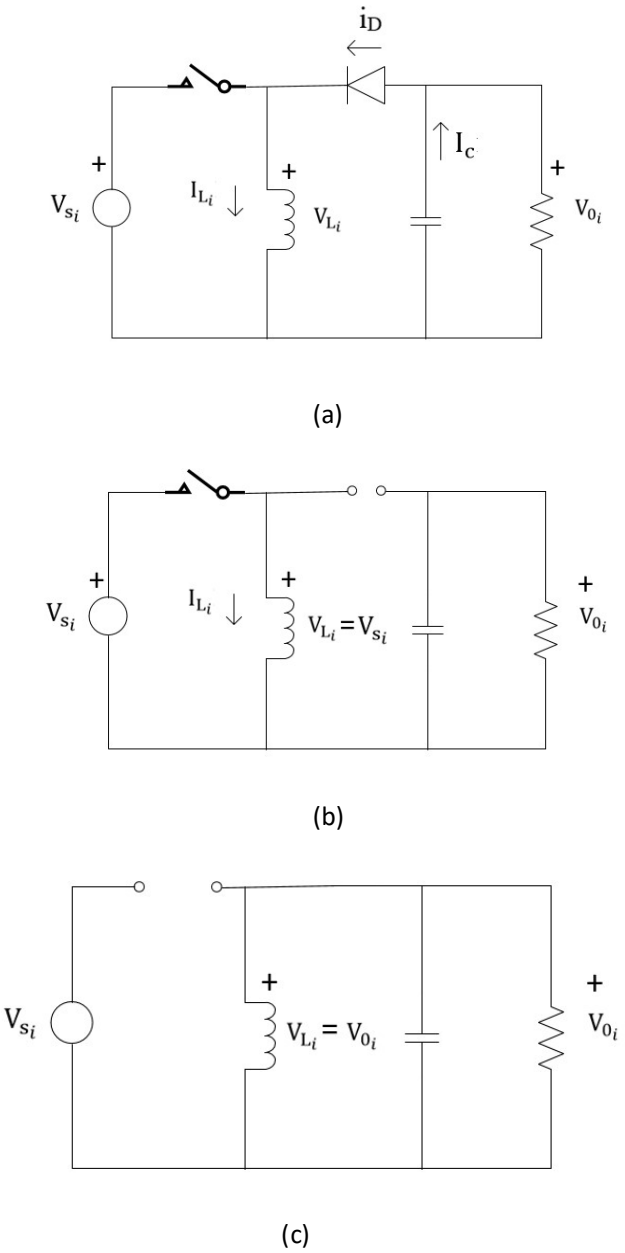

Fig.3.6: Buck-boost converter (a) Circuit; (b) Equivalent circuit for the switch closed; (c) Equivalent circuit for the switch open.

Analysis for the Switch Closed

When the switch is closed, the voltage across the inductor is

$$V_{L_i} = V_{s_i} = L_i \frac{di_{L_i}}{dt} \tag{3.16}$$

$$\frac{di_{L_i}}{dt} = \frac{V_{s_i}}{L_i} \tag{3.17}$$

The inductor current changes at a steady rate, suggesting that the current is increasing linearly. The preceding equation can be expressed as follows:

$$\frac{\Delta I_{L_i}}{\Delta t} = \frac{\Delta I_{L_i}}{DT} = \frac{V_{s_i}}{L_i} \tag{3.18}$$

Solving for ΔI_{L_i} when the switch is closed gives

$$(\Delta I_{L_i})_{cls} = \frac{V_{s_i} DT}{L_i} \tag{3.19}$$

Analysis for the Switch Open

While the switch is open, the current in the inductor cannot change rapidly, producing in a forward-biased diode and current into the resistor and capacitor. At this point, the voltage across the inductor is

$$V_{L_i} = V_{0_i} = L_i \frac{di_{L_i}}{dt} \tag{3.20}$$

$$\frac{di_{L_i}}{dt} = \frac{V_{0_i}}{L_i} \tag{3.21}$$

Inductor current changes at a constant rate, and current changes at a constant rate.

$$\frac{\Delta I_{L_i}}{\Delta t} = \frac{\Delta I_{L_i}}{(1-D)T} = \frac{V_{0_i}}{L_i} \tag{3.22}$$

Calculating for ΔI_{L_i},

$$(\Delta I_{L_i})_{open} = \frac{V_{0_i}(1-D)T}{L_i} \tag{3.23}$$

For steady-state operation, the net change in inductor current during a period must be zero. Using Eqs. (3.19), (3.20), and (3.21), (3.23),

$$(\Delta I_{L_i})_{cls} + (\Delta I_{L_i})_{open} = 0 \tag{3.24}$$

$$\frac{V_{s_i} DT}{L_i} + \frac{V_{0_i}(1-D)T}{L_i} = 0 \tag{3.25}$$

Solving for V_{0_i} ,

$$V_{0_i} = -V_{s_i}\left(\frac{D}{1-D}\right) \tag{3.26}$$

The needed duty ratio can be expressed as for particular input and output voltages:

$$D = \frac{|V_{0_i}|}{V_{s_i} + |V_{0_i}|} \tag{3.27}$$

For periodic operation, the average inductor voltage is zero, resulting in

$$V_{L_i} = V_{s_i}D + V_{0_i}(1 - D) = 0 \tag{3.28}$$

When you solve for Vo, you get the same conclusion as when you solve for Eq (3.26).

As demonstrated by equation, the output voltage has the opposite polarity as the source voltage (3.26). The output voltage of a buck-boost converter might be less than or more than the source voltage, depending on the duty ratio of the switch. If D 0.5, the output voltage is higher than the input voltage, and if D 0.5, the output voltage is lower. As a result, this circuit integrates the buck and boost converters' characteristics. However, polarity reversal on the output can be a disadvantage in some cases. Voltage and current waveforms are shown in Figure 3.7.

The supply is never explicitly connected to the load in a buck-boost converter. Energy is stored in the inductor when the switch is closed and given to the load when the switch is opened. A buck-boost converter is also known as an indirect converter as a result of this.

The power absorbed by the load must be equal to the power supplied by the source, where

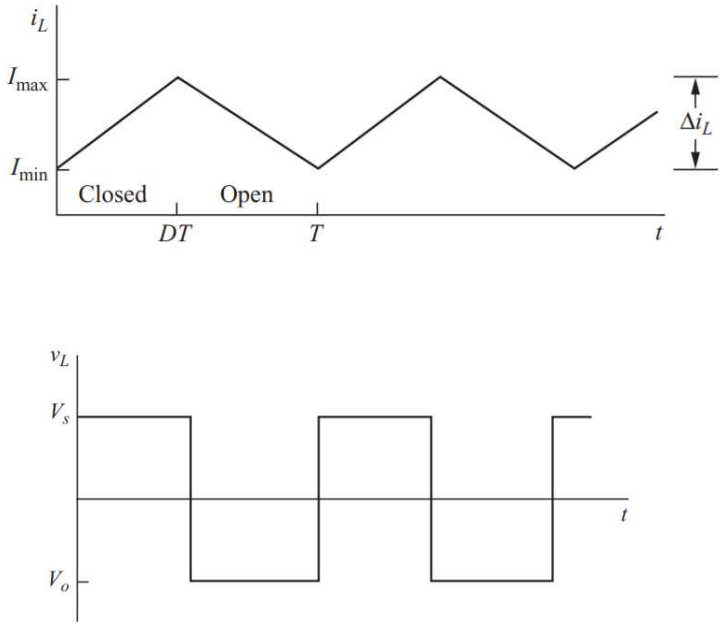

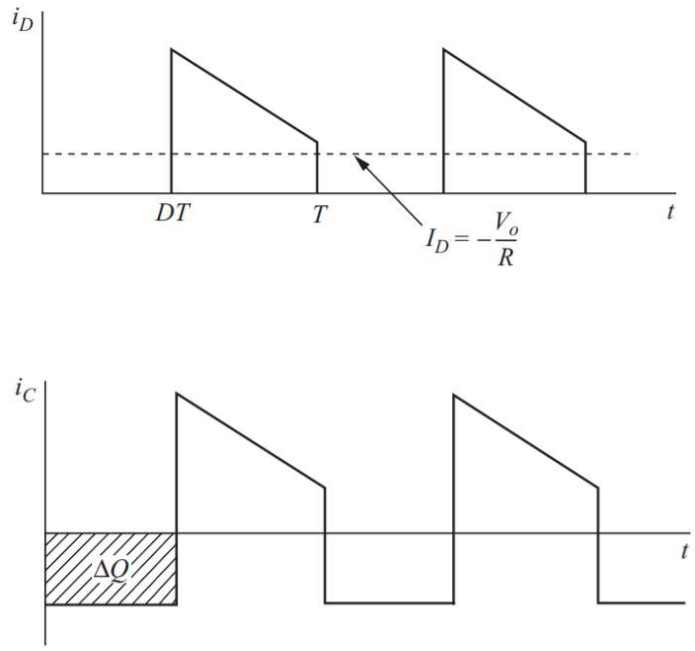

Fig.3.7: Buck-boost converter's waveforms. (a) Inductor current; (b) Inductor voltage; (c) Diode current; (d) Capacitor current.

$$P_{o_i} = \frac{V_{0_i}^2}{R} \tag{3.29}$$

$$P_{s_i} = V_{s_i} I_{s_i} \tag{3.30}$$

$$\frac{V_{0_i}^2}{R} = V_{s_i} I_{s_i} \tag{3.31}$$

The inductor's average current is proportional to the source's average current.

$$I_{s_i} = I_{L_i} D \tag{3.32}$$

Resulting in

$$\frac{V_{0_i}^2}{R} = V_{s_i} I_{L_i} D \tag{3.33}$$

Substituting for V_{0_i} using Eq. (3.26) and solving for I_{L_i}, we get

$$I_{L_i} = \frac{V_{0_i}^2}{V_{s_i} RD} = \frac{P_{o_i}}{V_{s_i} D} = \frac{V_{s_i} D}{R(1-D)^2} \tag{3.34}$$

Eqs. (3.19) and (3.12) are used to get the maximum and minimum inductor currents (3.34).

$$I_{max} = I_{L_i} + \frac{\Delta I_{L_i}}{2} = \frac{V_{s_i} D}{R(1-D)^2} + \frac{V_{s_i} DT}{2L_i} \tag{3.35}$$

$$I_{min} = I_{L_i} - \frac{\Delta I_{L_i}}{2} = \frac{V_{s_i} D}{R(1-D)^2} - \frac{V_{s_i} DT}{2L_i} \quad (3.36)$$

For continuous current to flow, the inductor current must remain positive. In Eq. (3.36), I_{min} is set to zero defining the border between continuous and discontinuous current.

$$(L_i fr)_{min} = \frac{(1-D)^2 R}{2} \quad (3.37)$$

$$L_{i_{min}} = \frac{(1-D)^2 R}{2fr} \quad (3.38)$$

Where f is the switching frequency.

Output Voltage Ripple

The output voltage ripple for the buck-boost converter is calculated using the capacitor current waveform in Fig. 3.7(d).

$$|\Delta Q_i| = \left(\frac{V_{0_i}}{R}\right) DT = C\Delta V_{0_i} \quad (3.39)$$

Solving for ΔV_{0_i}

$$\Delta V_{0_i} = \frac{V_{0_i} DT}{RC} = \frac{V_{0_i} D}{RCF} \quad (3.40)$$

$$\frac{\Delta V_{0_i}}{V_{0_i}} = \frac{D}{RCF} \quad (3.41)$$

Like other converters, the equivalent series resistance of the capacitor can have a significant impact on the output ripple voltage. The peak-to-peak variation in capacitor current is the same as the highest inductor current. Using the capacitor model depicted in WhereI_{Lmax} , is calculated using Eq (3.35),

$$\Delta V_{0_i,ESR} = \Delta I_c r_c = I_{L_i max} r_c \quad (3.42)$$

3.4. Design of DC-AC Converter

Grid-connected inverters serve as a link between the solar PV array and the utility. Because of its small size, low cost, and improved efficiency, transformer less inverters have recently become popular in single phase systems. In transformer less inverters, however, there is a leakage current problem, which can be mitigated via inverter topologies and modulation techniques.

Based on their leakage current performance and decoupling approach, topologies can be categorized in three ways.

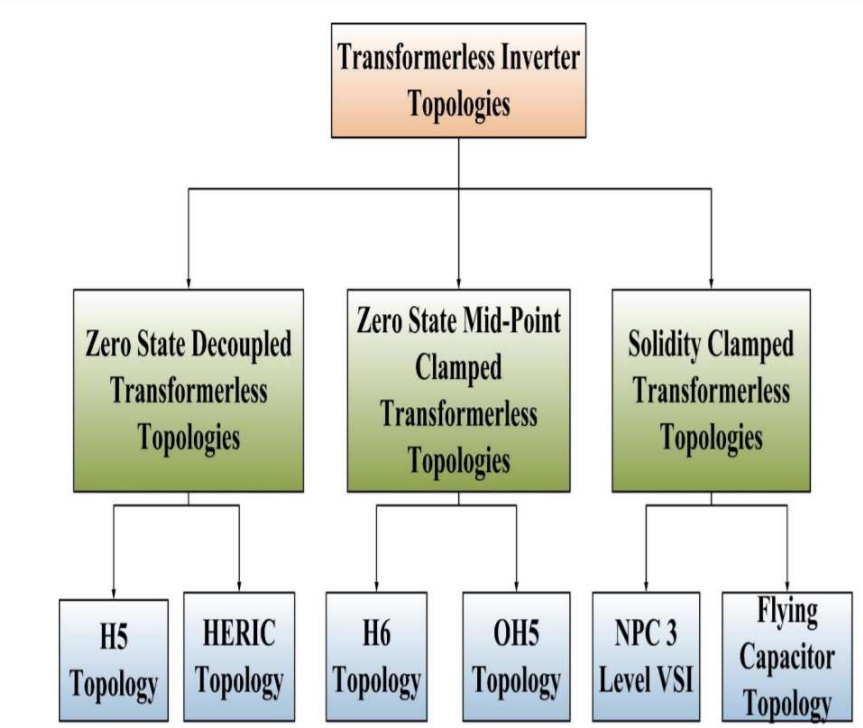

Fig. 3.8: Classification of Single Phase Transformer-less Inverter Topologies

Table 3.2: Transformer-less Inverter Topologies Comparative Analysis

	Transformerless topologies	**Input Capacitor**	**Switches**	**Diodes**	**Leakage Current**
Zero-state decouple transformerless topologies	H5 topology	1	5	0	Medium
	HERIC topology	1	6	0	Very Low
Zero-state mid-point clamped transformerless topologies	H6 topology	2	6	2	Low
	oH5 topology	2	6	0	Medium
Solidity clamped transformerless topologies	NPC three-level VSI	2	4	2	Low
	Flying capacitor topology	3	4	0	Low

3.4.1. Basic designing of Full Bridge Converter

The primary circuit for converting dc to ac is the full-bridge converter depicted in Fig. 3.9(a). In this application, an ac output is synthesised from a dc input by closing and opening the switches in the correct order. The output voltage V (0 i) can be Vdc, -Vdc, or zero depending on which switches are closed. Figure 3.9(b) to (d) shows comparable circuits for switch combinations (e).

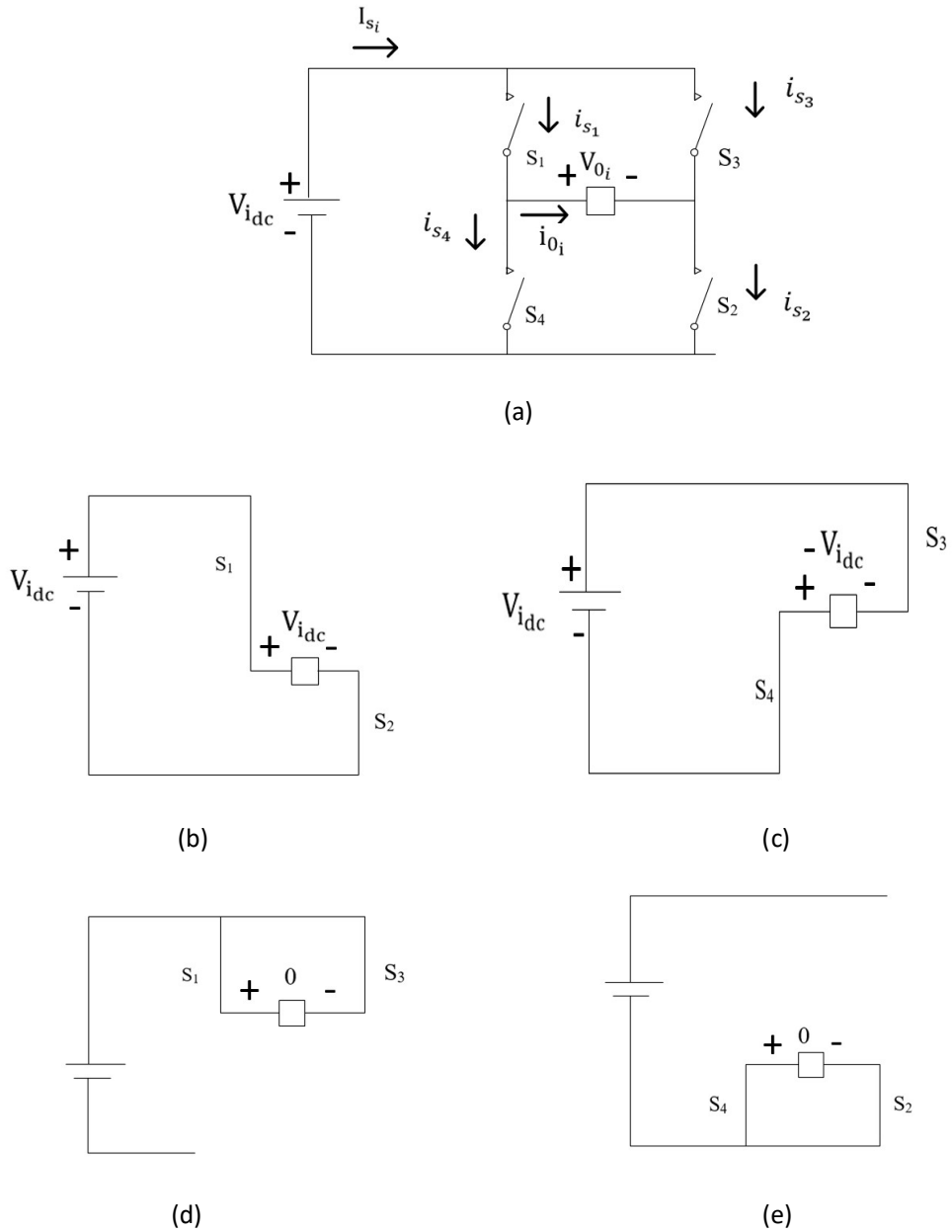

Fig.3.9: (a) Full-bridge converter; (b) S1 and S2 closed; (c) S3 and S4 closed; (d) S1 and S3 closed; (e) S2 and S4 closed.

It is not recommended that S1 and S4, as well as S2 and S3, be closed at the same time. Otherwise, a short circuit would develop across the dc source. Switching transition delays must be handled in the switch control since real switches do not turn on or off quickly. If the switch "on" times overlap, a short circuit, also known as a shoot through fault, will form across the dc voltage source. The amount of time allowed for transition is referred to as "blanking time."

The simplest switching approach in a full-bridge converter produces a square wave output voltage. The load is linked to Vdc when S1 and S2 are closed, and when S3 and S4 are closed, the load is connected to Vdc. When the load voltage is cycled between Vdc and Vdc on a regular basis, a square wave voltage is produced across the load. Despite the non-sinusoidal nature of this alternating output, it may be sufficient for some applications.

For a series RL load with a square wave output voltage, assume switches S1 and S2 in Fig. 3.9(a) close at t = 0. When the voltage across the load reaches Vdc, current in the load, as well as in S1 and S2, begins to increase. The current is the sum of all forced and natural responses.

$$i_{0_i}(t) = i_{fr}(t) + i_n(t)$$

$$= \frac{V_{i_{dc}}}{R} + Ae^{\frac{-t}{T}} \text{ for } 0 \le t \le \frac{T}{2} \qquad (3.43)$$

T = L/R, where A is a constant calculated from the initial situation.

At t = T/2, S1 and S2 open, while S3 and S4 close. The voltage across the RL load is Vdc, and the current is type

$$i_{0_i}(t) = \frac{-V_{i_{dc}}}{R} + Be^{\frac{-(t-\frac{T}{2})}{T}} \text{ for } \frac{T}{2} \le t \le T \qquad (3.44)$$

Using the initial condition as a starting point, the constant B is determined.

When the circuit is first activated and the initial inductor current is zero, a transient occurs before the load current reaches a steady-state condition. In steady state, io is periodic and symmetric about zero, as shown in Fig. 3.10. Allow I min to be the beginning condition for the current described in Eq(3.43) and Imax to be the initial condition for the current described in Eq(3.43) (3.44).

At t = 0, evaluate Eq. (3.43)

$$i_{0_i}(0) = \frac{V_{i_{dc}}}{R} + Ae^0 = I_{min} \tag{3.45}$$

or

$$A = I_{min} - \frac{V_{i_{dc}}}{R} \tag{3.46}$$

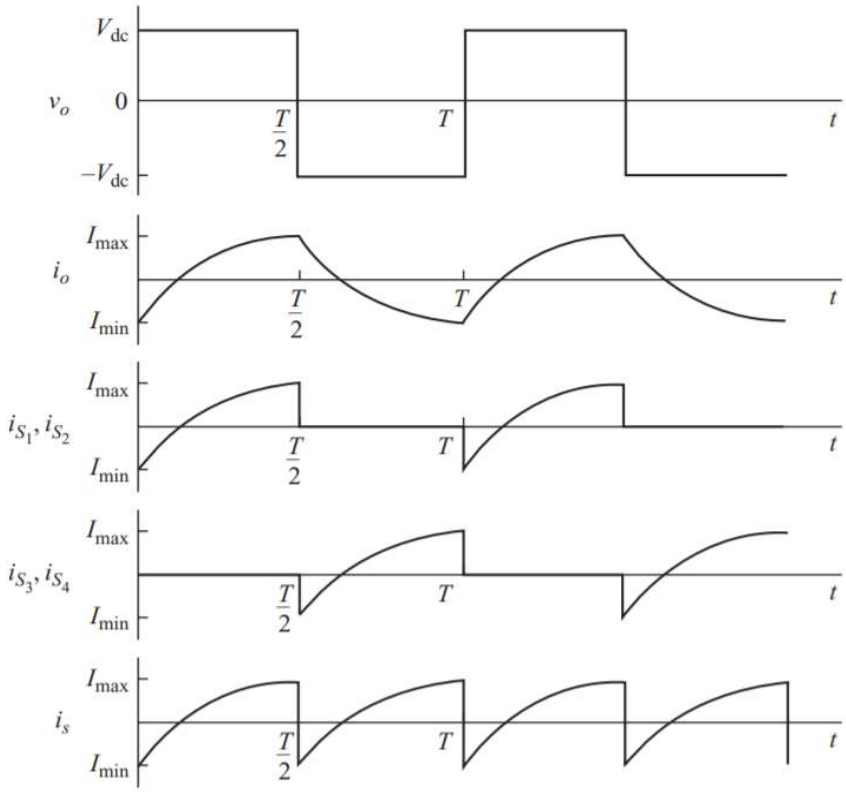

Fig.3.10: output voltage and steady-state current waveform with RL Load

Eq. (3.44) is however evaluated at t = T2.

$$i_{0_i}\left(\frac{T}{2}\right) = \frac{-V_{i_{dc}}}{R} + Be^0 = I_{max} \tag{3.47}$$

or

$$B = I_{max} + \frac{V_{i_{dc}}}{R} \tag{3.48}$$

The current waveforms represented by Eqs. (3.43) and (3.44) become stable in steady state.

$$i_{0_i}(t) = \begin{cases} \frac{V_{i_{dc}}}{R} + \left(I_{min} - \frac{V_{i_{dc}}}{R}\right) e^{\frac{-t}{T}} & \text{for } 0 \le t \le \frac{T}{2} \\ \frac{-V_{i_{dc}}}{R} + \left(I_{max} + \frac{V_{i_{dc}}}{R}\right) e^{\frac{-(t-\frac{T}{2})}{T}} & \text{for } \frac{T}{2} \le t \le T \end{cases} \quad (3.49)$$

Evaluating the first half of Eq. (3.49) at t =T/2 yields an expression for I_{max}.

$$i_i\left(\frac{T}{2}\right) = I_{max} = \frac{V_{i_{dc}}}{R} + \left(I_{min} - \frac{V_{i_{dc}}}{R}\right) e^{\frac{-t}{2T}} \quad (3.50)$$

and by symmetry,

$$I_{min} = -I_{max} \quad (3.51)$$

Eq. (3.50) is solved for Imax by substituting I_{max} for I_{min}

$$I_{max} = -I_{min} = \frac{V_{i_{dc}}}{R}\left(\frac{1-e^{\frac{-T}{2T}}}{1+e^{\frac{-T}{2T}}}\right) \quad (3.52)$$

Eqs. (3.49) and (3.52) explain the current in an RL load in the steady state when a square wave voltage is supplied. Figure 3.9 depicts the currents in the load, source, and switches.

$$I_{rms} = \sqrt{\frac{1}{T}\int_0^T {i_i}^2(t)d(t)} = \sqrt{\frac{2}{T}\int_0^{T/2}\left[\frac{V_{i_{dc}}}{R} + \left(I_{min} - \frac{V_{i_{dc}}}{R}\right) e^{\frac{-t}{T}}\right]^2 dt} \quad (3.53)$$

If the switches are optimal, the power delivered by the source must be equal to the power absorbed by the load. A dc source's output power is calculated using

$$P_{i_{dc}} = V_{i_{dc}} I_s \quad (3.54)$$

3.5. PWM Techniques

By altering the duty cycle of the PWM signal, which results in an AC signal, it is possible to obtain a certain voltage pattern across the electrical load. A low pass filter is required to obtain a smooth sinusoidal wave from the PWM output. A PWM control signal can be generated using an analogue comparator or a digital microcontroller.Both methods are widely utilized in the industry to generate sinusoidal PWM signals and obtain sinusoidal inverter output. In the discipline of power electronics, a PWM signal has a wide range of applications. Some of the reasons for its use are as follows:

• Power loss is significantly decreased - When switches are left on or off for an extended period of time, there is extremely little conduction power loss across the associated switches.

• PWM signal generation is uncomplicated - especially in the digital arena, PWM signal generation has become quite simple. Many microcontrollers include hardware that can handle and produce PWM waves, so the controller does not need to worry about it.

• D/A conversion - Controlling the output signal solely by the duty cycle considerably improves this technique, making it suitable for digital to analogue signal conversion. Controlling the duty cycle, for example, can change the speed of an electronic DC motor.

3.5.1. Unipolar SPWM

This modulation scheme normally just requires two sinusoidal waveforms of amplitude Vm and -Vm, both of which have the same amplitude but are 180 degrees out of phase with each other. Two sinusoidal waves are compared to a triangular carrier waveform Vc in the diagram above, yielding gating signals Vg1 and Vg2 for the two legs' uppermost switches. Two upper switches are not switched on at the same time, as is the case with bipolar SPWM, when two switches are constantly turned on at the same time. It's called unipolar SPWM because the output voltage swings between zero and +Vd for the positive half cycle and zero and Vd for the negative half cycle. The unipolar PWM inverter has less electromagnetic interference and switching loss than the bipolar PWM inverter. The efficiency of unipolar switching is higher than that of its counterpart.

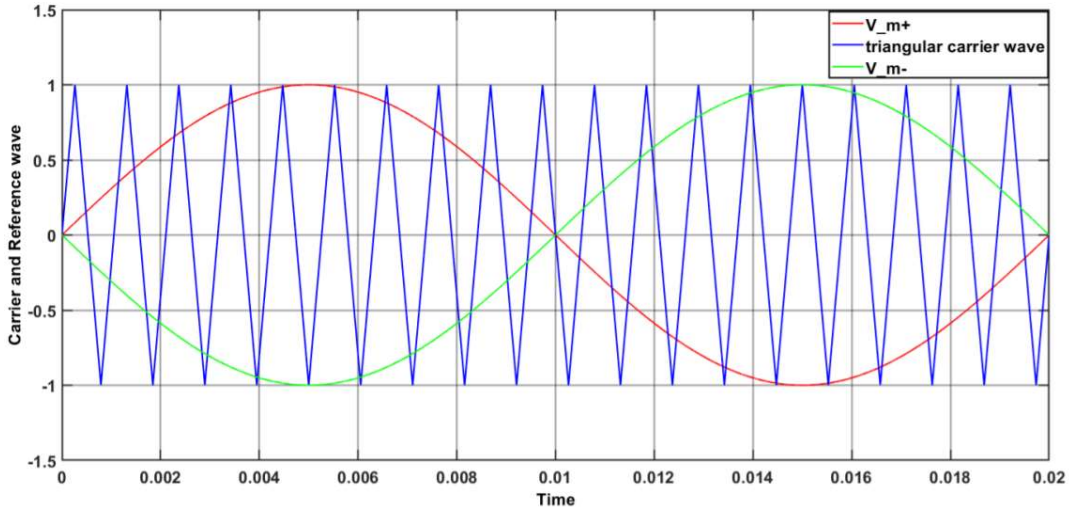

Fig.3.11: Unipolar SPWM waveform

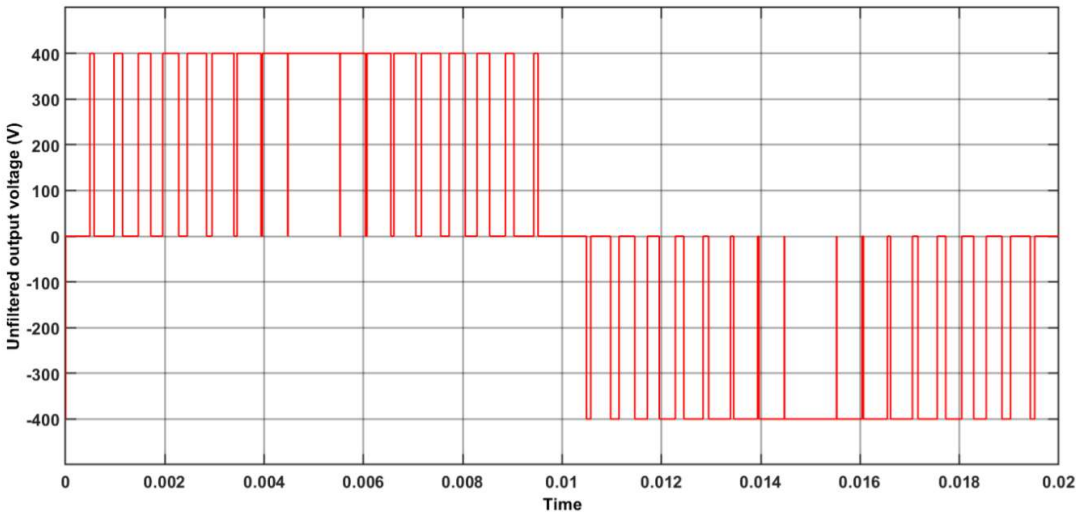

Fig.3.12: Inverter output voltage with Unipolar SPWM

3.5.2. Bipolar SPWM

In this technique, the upper and lower leg switches do not turn on and off at the same moment, but rather in a complementary manner. As a result, just two gating signals, Vg1 and Vg2, must be managed, and they are created by comparing one sinusoidal wave Vm with a triangular carrier wave Vc. It's called bipolar SPWM because the inverter's output voltage alternates between +Vd and Vd for both half cycles.

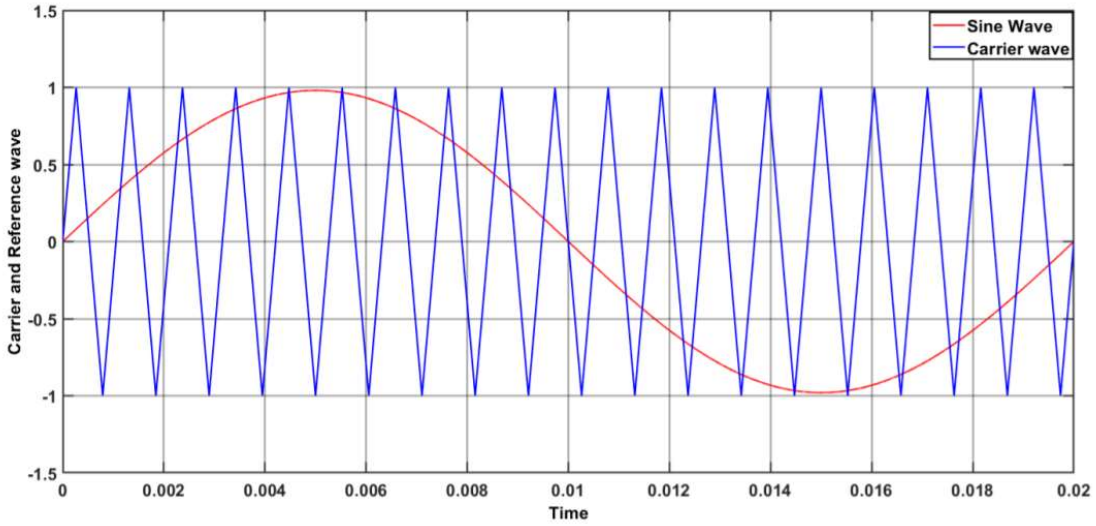

Fig.3.13: Bipolar SPWM waveform

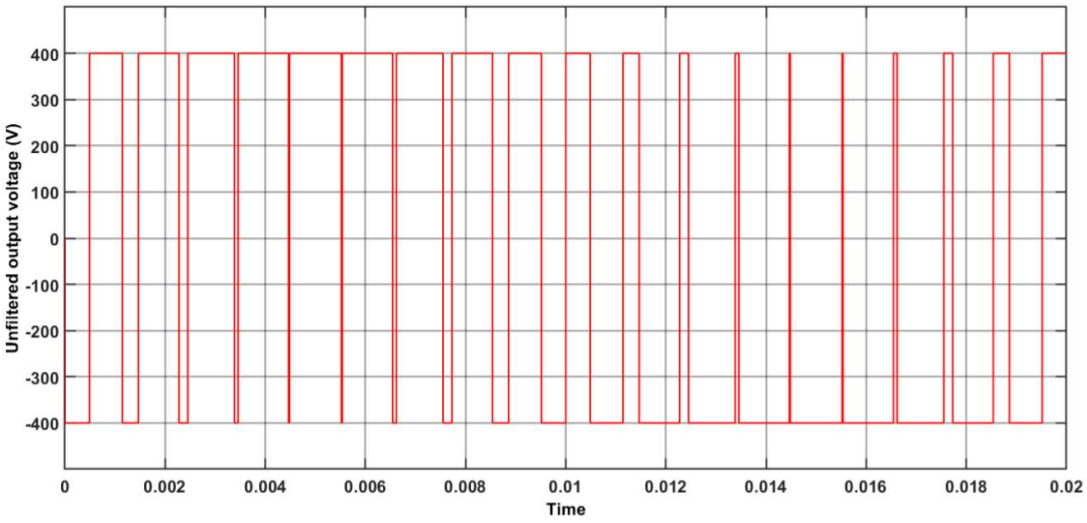

Fig.3.14: Inverter output voltage with Bipolar SPWM

3.6. Working Principle of the Dual Buck & Boost based Inverter (DBBI)

As illustrated in the design in Fig. 1, the suggested Dual Buck & Boost based Inverter (DBBI) has a dc to dc converter step followed by an inverting stage. To service the solar PV array's two subarrays, PV1 and PV2, the dc to dc converter stage consists of two CONV1 and CONV2 dc to dc converter segments. The CONV1 segment consists of the self-commutated switches Q1 and D1, the anti-parallel body diodes Df1, Df3, the freewheeling diodes Df1, Df3, and the filter inductors and capacitors L1, Cf1, and Cf3.

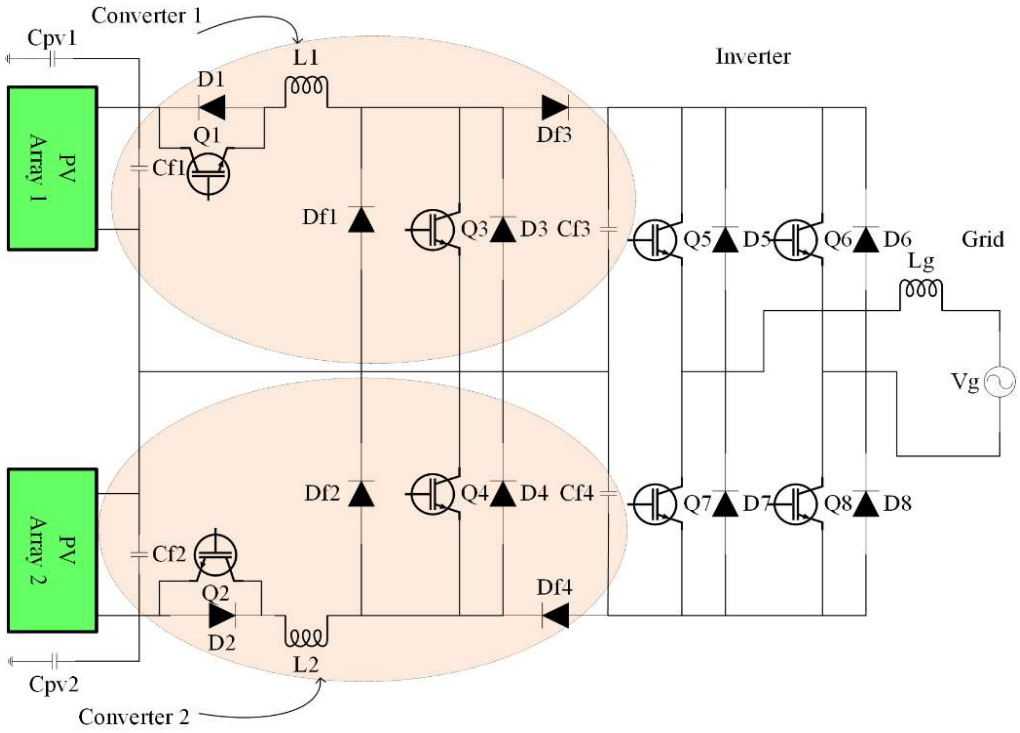

Fig 3.15: Dual Buck & Boost based Inverter (DBBI).

Self-commutated switches, Q2 and Q4, anti-parallel body diodes, D2, and D4, freewheeling diodes, Df2, Df4, and filter inductors and capacitors, L2, Cf2, and Cf4, make up the CONV2 sector. The inverting stage is made up of self-commutated switches S5, S6, S7, and S8, as well as their associated body diodes D5, D6, D7, and D8. The filter inductor, Lg, connects the grid to the inverter stage. Two capacitors, Cpv1 and Cpv2, approximate the parasitic capacitance of the PV array to the ground.

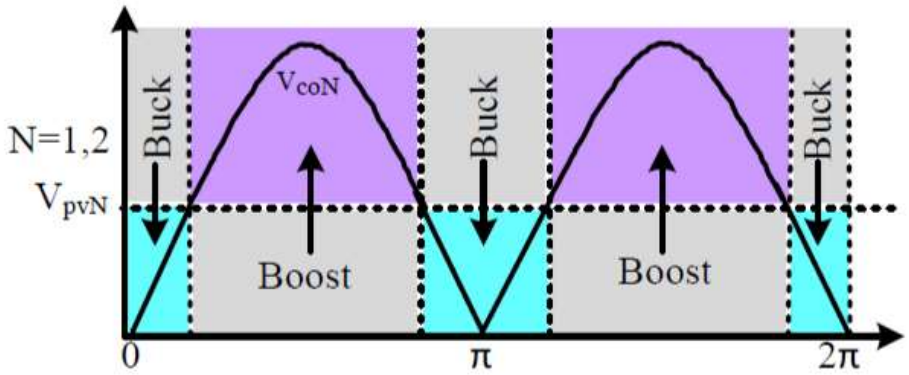

Fig. 3.16: Buck stage and Boost stage of the proposed inverter.

Whenever Vpv1 ≥ vcf3, CONV1 operates in buck mode, whereas when Vpv2 ≥ vcf4, CONV2 operates in buck mode. The MPP voltages of PV1 and PV2 are Vpv1, Vpv2, and the output voltages of CONV1 and CONV2 are vcf3, vcf4, respectively. During the buck mode duty ratios of the switches, S1 and S2 are adjusted sinusoidally to guarantee sinusoidal grid current (ag), while S3 and S4 are turned off. When Vpv1< vcf3, CONV1 is in boost mode, while CONV2 is in boost mode when Vpv1< vcf3. During boost mode, the duty ratios of the switches S3 and S4 are altered sinusoidally to ensure sinusoidal ig, whereas S1 and S2 remain on.

The sinusoidal switching pulses of the switches of CONV1 and CONV2 are matched with the grid voltage, vg, to ensure unity power factor working. Switches S5 and S8 are kept on and switches S6 and S7 are kept off permanently during the positive half cycle (PHC), whereas switches S6 and S7 are kept on and switches S5 and S8 are kept off permanently during the negative half cycle (NHC).

Two switches Q1 and Q3, as well as two diodes D1 and D3, are always cycling in the buck boost converter 1 operation mode. When Q3 is off and D3 is conducting, a positive buck–boost converter can be used as a buck converter by manipulating switch Q1 and diode D1. While Q1 is on and D1 is not conducting, it can also function as a boost converter by regulating switch Q3 and diode D3. When the battery voltage exceeds the output reference voltage, the converter becomes a buck converter. When the battery voltage falls below the output reference voltage, the converter should automatically adjust to boost mode.

The single-phase inverter is connected to the output terminals of converters 1 and 2. Four power semiconductor switches Q5, Q6, Q7, and Q8 are anti-parallel with diodes D5, D6, D7, and D8 in the single-phase inverter. The inverter's output terminal is connected to the 230v, 50 Hz grid via the filter inductor Lg.

3.7. Control Algorithm

Figure 3.17 depicts the control algorithm for the proposed double stage single phase grid linked PV system.

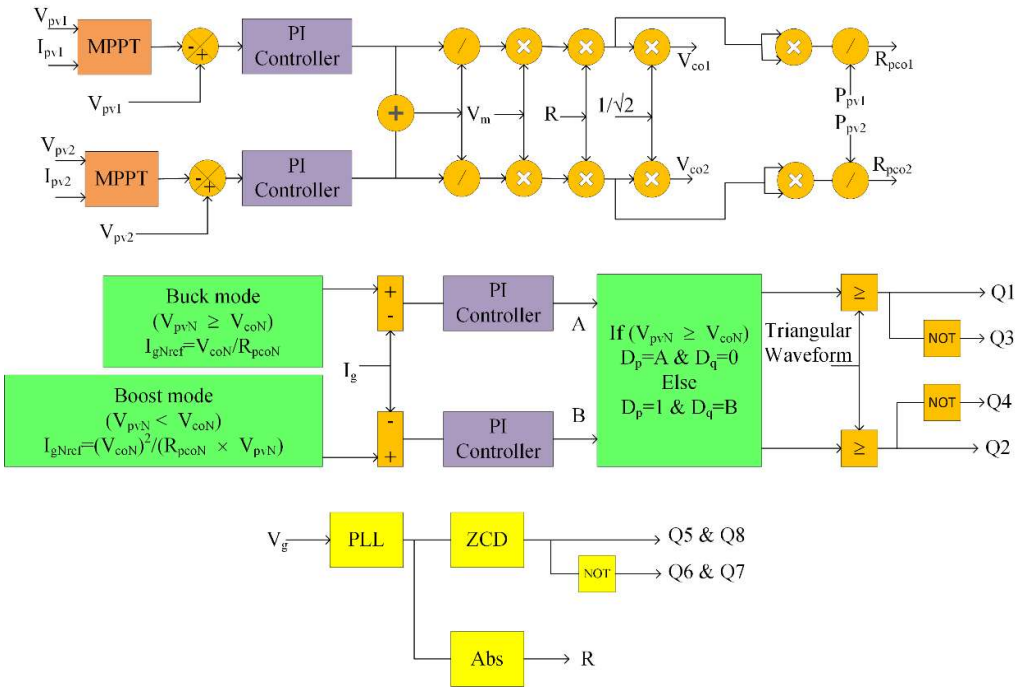

Fig. 3.17: Control logic of the proposed system

The MPPT algorithm takes two inputs: PV voltage and current, and provide reference voltage for the next stage. The MPPT's output is compared to the voltage of the PV array. This error voltage is processed through a PI controller to provide a control signal, which is then processed through a series of stages to produce the control outputs V_{co1} & V_{co2}, R_{pco1} & R_{pco2}.

$$V_{coNm} = \frac{P_{pvN}}{P_{pv1}+P_{pv2}} \times V_m \times R \tag{3.55}$$

$$V_{coN} = V_{coNm} \times \frac{1}{\sqrt{2}} \tag{3.56}$$

$$R_{pcoN} = \frac{{V_{coNm}}^2}{P_{pvN}} \tag{3.57}$$

Where, N= 1 & 2, P_{pv1} is the first PI controller's control output, P_{pv2} is the second PI controller's control output, V_m is the grid voltage's peak amplitude, and R is the absolute value instantaneous grid voltage.

The current reference signal is generated using the converter's buck and boost modes. If PV voltage V_{pvn} is greater than equal to V_{coN} than current reference is generated based on following equation,

$$I_{gNref} = \frac{V_{coN}}{R_{pcoN}} \tag{3.58}$$

If PV voltage V_{pvn} is less than to V_{coN} than current reference is generated based on following equation,

$$I_{gNref} = \frac{{V_{coN}}^2}{R_{pcoN} \times V_{pvn}} \tag{3.59}$$

The grid current I_{LN} is compared to the current reference (I_{gNref}). Two PI controllers process the error current, and the PI controllers generate two control signals, A and B.

If PV voltage V_{pvn} is greater than equal to V_{coN} than duty cycle for converter 1 is set to A and duty cycle for converter 2 is set to zero else duty cycle for converter 1 is set to one and duty cycle for converter 2 is set to B. To create pulses for the switches Q1 & Q3 and Q2 & Q4, the duty cycle is checked to a triangle wave. The grid side inverter switching pulse is generated using the grid voltage, which is processed using a phase locked loop and a zero crossing detection circuit to generate pulses with grid frequency. These pulses are given to switches Q5, Q6, Q7 and Q8. Q5 & Q8 is tuned on at same time and Q6 & Q7 is tuned on at same time based on grid cycle.

The dual buck boost converter inductor & capacitor, grid filter inductor is calculated using following equation,

$$L_N = \frac{V_{pvN}}{4 \times \Delta I_{LN} \times F_s} \tag{3.60}$$

$$C_{oN} = \frac{x \times P_{pvN}}{2\pi \times F_g \times V_{coN}^2} \tag{3.61}$$

Where, F_s is the dual buck-boost converter switching frequency, F_g is the frequency of the grid, ΔI_{LN} is the ripple inductor current and it is taken as 15 % of the rated current at peak and x is the loading factor and it taken as 2.5 %. Grid filter inductor value is selected less than converter 1 inductor value for improving stability margin.

Table 3.3 lists the specifications for the twin buck-boost converter and grid inverter.

Table 3.3 Specification of converter and inverter

PARAMETER	VALUES
CONVERTER	
POWER RATING	700 WATTS
INDUCTOR (L_1)	0.6 mH
INDUCTOR (L_2)	0.1 mH
CAPCITOR (C_{f1} & C_{f2})	1 μF
CAPCITOR (C_{f3} & C_{f4})	5 μF
CAPCITOR (C_{pv1} & C_{pv2})	0.1 μF
SWITCHING FREQUENCY	5 kHz
INVERTER	
POWER RATING	800 WATTS
GRID SIDE INDUCTOR (L_g)	0.4 mH
CONTROLLER GAINS	
VOLTAGE CONTROLLER -PROPORTIONAL GAIN	0.32 & 0.56
CURRENT PI CONTROLLER	0.5 & 1.32

3.8. Conclusion

This chapter covers the essential components of a grid-connected PV system, as well as the Dual buck boost inverter for solar PV integration with single phase grid. Various single phase transformer less inverter topologies, as well as types of DC-DC converters and basic Buck-Boost converter design, were identified and addressed. Various PWM approaches are also investigated. This chapter explains the control method for obtaining the maximum power point from a solar PV array, as well as the voltage and current control technique for single-phase grid integration.

CHAPTER 4

Maximum Power Point Tracking (MPPT) algorithms

4.1. General

This chapter explains about different MPPT algorithms for solar PV systems. The conventional MPPT algorithm such as fixed voltage method, perturb and observe method, incremental conductance method and proposed fuzzy logic based MPPT algorithm have been discussed in this chapter elaborately.

4.2. Fixed Voltage Maximum Power Point algorithm

The voltage across the solar PV panel is kept at a fixed reference voltage in the Fixed Voltage MPPT algorithm, which is based on the voltage at MPPT of the PV panel's PV characteristics. The fixed PV voltage MPPT concept is depicted in the Figure 4.1.

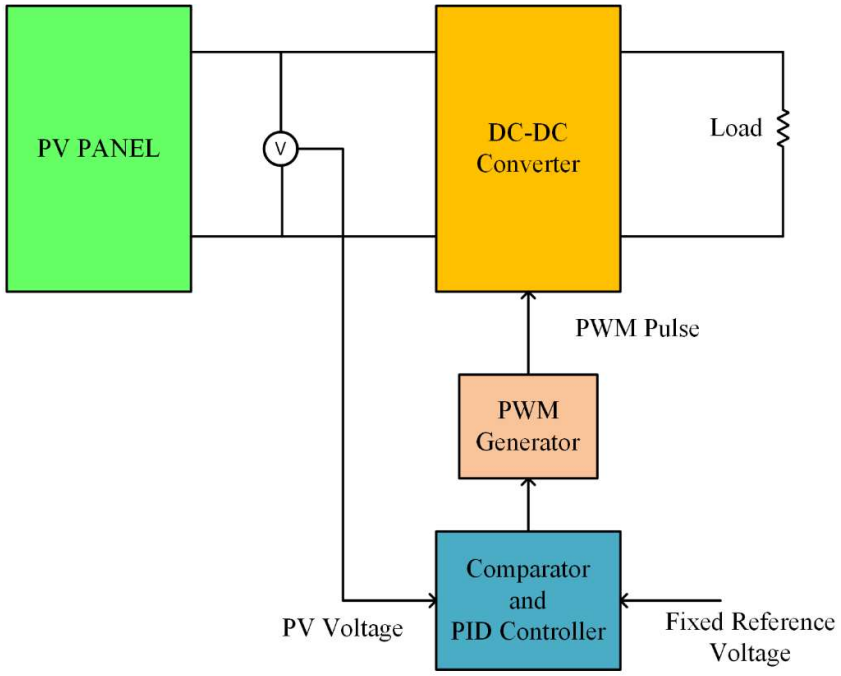

Fig 4.1: Fixed Voltage MPPT for Solar PV system

In this method, PV panel voltage is measured using voltage sensor and it is compared with fixed voltage reference i.e., voltage at MPPT of the PV panel. A Proportional Integral Derivative (PID) controller is used to process the error voltage. The PID controller generate the control signal i.e., duty cycle based on this error voltage. The duty is processed via PWM generator. In PWM generator, duty is compared with

triangular wave and it generates the PWM pulse. The power semiconductor switches in the DC-DC converter are turned on and off by this PWM pulse. The PV panel's maximum power is retrieved based on the switching pulse and duty cycle.

Let consider PV voltage is denoted by V_{pv} , Fixed reference voltage is denoted by V_f and error voltage expressed by following equation,

$$e(t) = V_f - V_{pv} \tag{4.1}$$

This error voltage is processed via PID controller and expression for the PID controller output is given by,

$$u(t) = K_p \times e(t) + K_i \int e(t)dt + K_d \frac{de(t)}{dt} \tag{4.2}$$

Where, K_p is the PID controller's proportional gain, K_i is the PID controller's integral gain and K_d is the PID controller's derivative gain. These controller gain can be obtained by conventional tuning method such Ziegler Nichols Method or can be tuned by optimization algorithm.

The controlled output from the PID controller is processed via PWM generator i.e., controlled output or duty cycle is compared with triangular waveform. Let considered $T(t)$ instantaneous amplitude for the triangular waveform and PWM generator action can be expressed by the following equation,

$$\begin{gathered} if\ u(t) > T(t) \\ Pulse = 1 \\ else \\ Pulse = 0 \end{gathered} \tag{4.3}$$

The reference fixed voltage can be chosen by performing the following steps: first, as illustrated in Figure 4.2, determine the current voltage and power voltage characteristics of the PV panel under various irradiance situations.

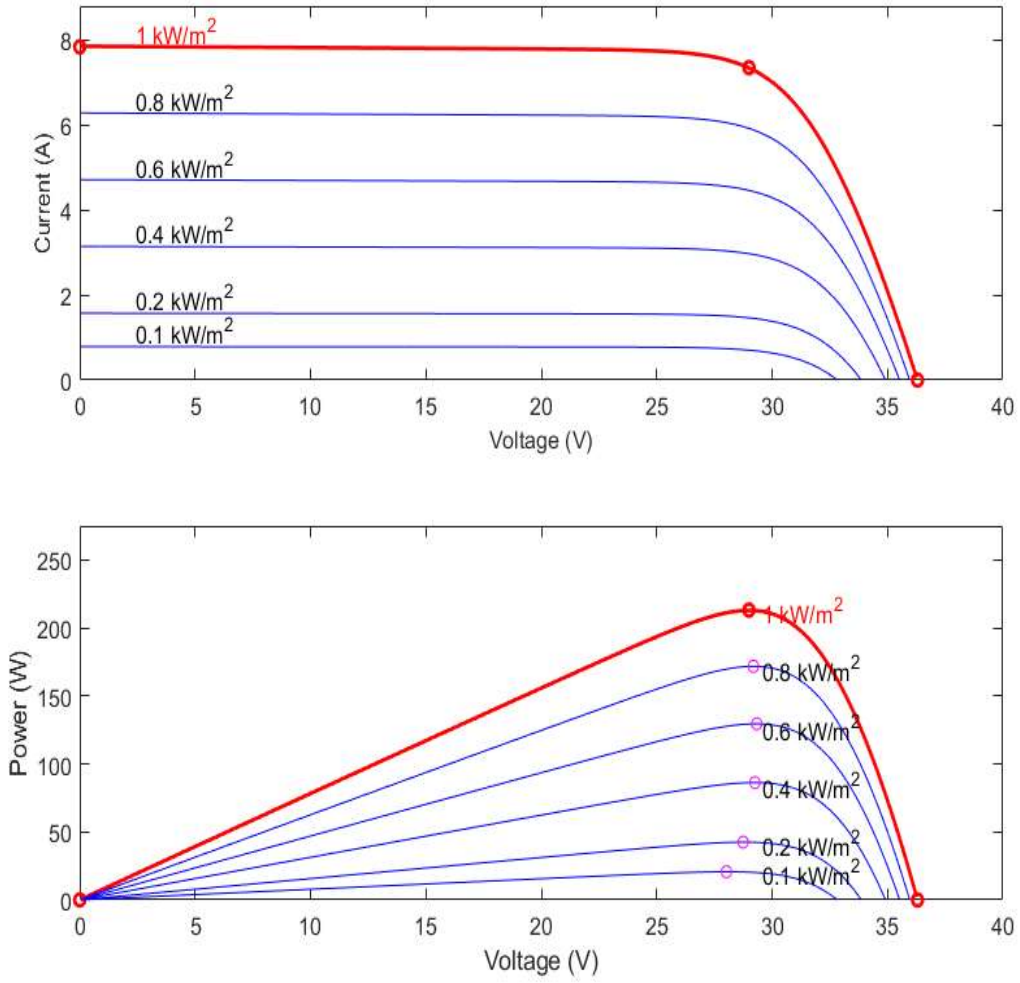

Fig 4.2: Current-voltage, Power -voltage characteristics of the typical PV panel.

The problem with this system is that when cell temperature varies dramatically, precise tracking of the solar PV panel's maximum power is impossible.

4.3. Perturb and Observe Maximum Power Point algorithm

The Perturb and Observe MPPT algorithm maintains the voltage across the solar PV panel at the MPPT of the PV panel's PV characteristics based on PV current and PV voltage. Figure 4.3 depicts the Perturb and Observe MPPT algorithm concept.

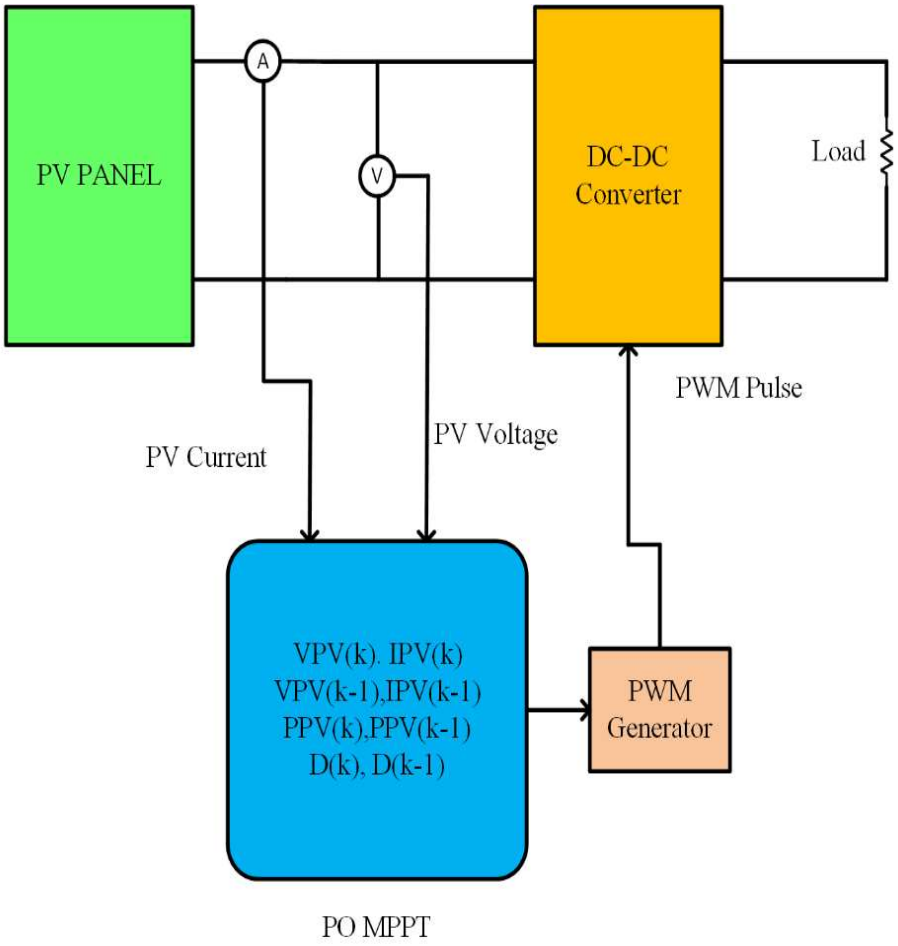

Fig 4.3: Perturb and Observe MPPT technique for Solar PV system.

PV voltage and current are measured using a voltage and current sensor in this manner. After that, one sample is added to the voltage and current to acquire the previous sample value for PV voltage and current. The present instant PV voltage and current, as well as the prior instant voltage and current, are used to determine the change in power. Changes in power and voltage circumstances determine the duty from the PO MPPT. The power-voltage characteristics of the PV panel are used to describe how the PO MPPT works.

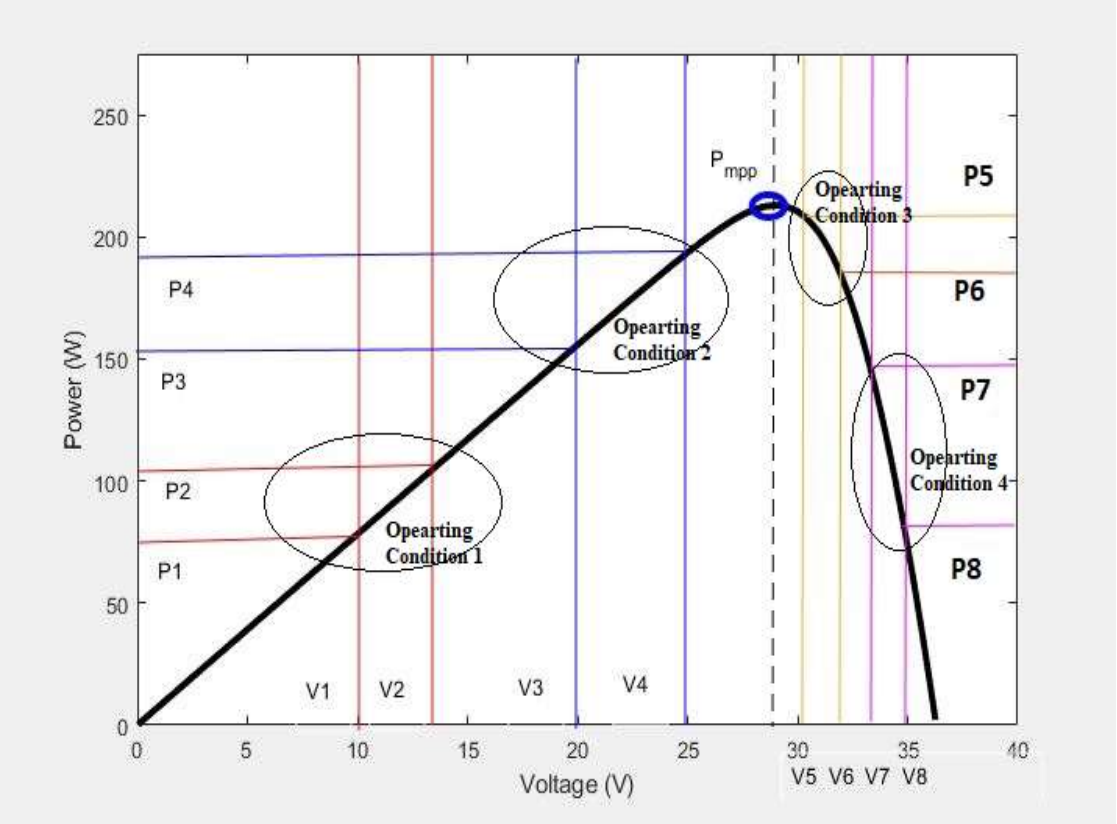

Fig 4.4: Power-Voltage characteristics of typical PV Panel

Figure 4.4 depicts the power-voltage characteristics of the typical PV panel. There are four operating conditions are considered for explain the PO MPPT algorithm and it is indicated in different color such as first operating point indicated in red, second operating point indicated in blue, third operating point indicated in brown and fourth operating point indicated in pink in the Figure 4.4.

Case 1: Consider first operating point, PV voltage change from V1 to V2 and Power of the PV panel is change from P1 to P2. The sign of change in power (P2-P1) and sign of change in voltage (V2-V1) is positive during these conditions, PV voltage should be increased from V2 to some other value to shift the power point towards the maximum power point of the PV panel.

$$if\ (P2 - P1 > 0)\ \&\&\ (V2 - V1 > 0)$$
$$\{V_{PV} = V2 + \Delta V\} \tag{4.4}$$

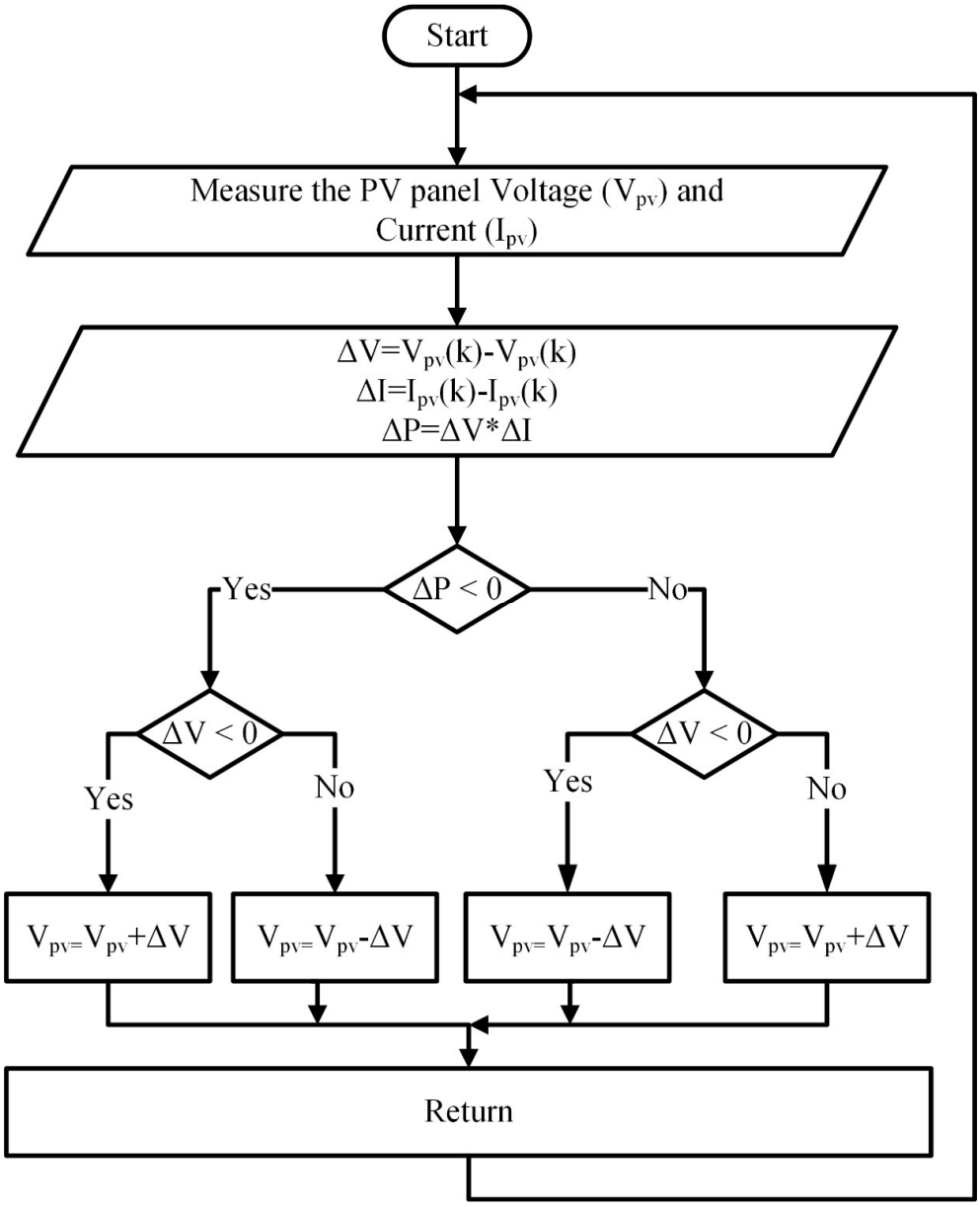

Fig 4.5: Flow Chart for PO MPPT

Case 2: Consider second operating point, PV voltage is change from V4 to V3 and PV power of the change from P4 to P3. During these conditions, the sign of change in power (P3-P4) is negative, and the sign of change in voltage (V3-V4) is negative, therefore PV voltage should be increased from V3 to another number to shift the power point closer to the PV panel's maximum power point.

$$if\ (P3 - P4 < 0)\ \&\&\ (V3 - V4\ < 0)$$
$$\{V_{PV} = V3 + \Delta V\} \tag{4.5}$$

Case 3: Consider third operating point, PV voltage is change from V5 to V6 and PV power of the change from P5 to P6. During these conditions, the sign of change in power (P6-P5) is negative, while the sign of change in voltage (V6-V5) is positive, hence PV voltage should be reduced from V6 to a lower value to move the power point closer to the PV panel's maximum power point.

$$if\ (P6 - P5 < 0)\ \&\&\ (V6 - V5\ > 0)$$
$$\{V_{PV} = V6 - \Delta V\} \tag{4.6}$$

Case 4: Consider fourth operating point, PV voltage is change from V8 to V7 and PV power of the change from P8 to P7. During these conditions, the sign of change in power (P7-P8) is positive and the sign of change in voltage (V7-V8) is negative, hence PV voltage should be reduced from V7 to another number to move the power point closer to the PV panel's maximum power point.

$$if\ (P7 - P8\ > 0)\ \&\&\ (V7 - V8\ < 0)$$
$$\{V_{PV} = V7 - \Delta V\} \tag{4.7}$$

Figure 5.6 depicts the flow chart of the PO MPPT algorithm based on these four operating circumstances. The difficulty with this method is that it oscillates about the PV panel's maximum power point and takes a long time to follow the maximum power point.

4.4 Incremental Conductance Maximum Power Point algorithm

The incremental conductance MPPT algorithm maintains the voltage across the solar PV panel at the maximum power point of the PV panel's PV characteristics based on PV current and PV voltage. Figure 4.6 depicts the incremental conductance MPPT algorithm concept.

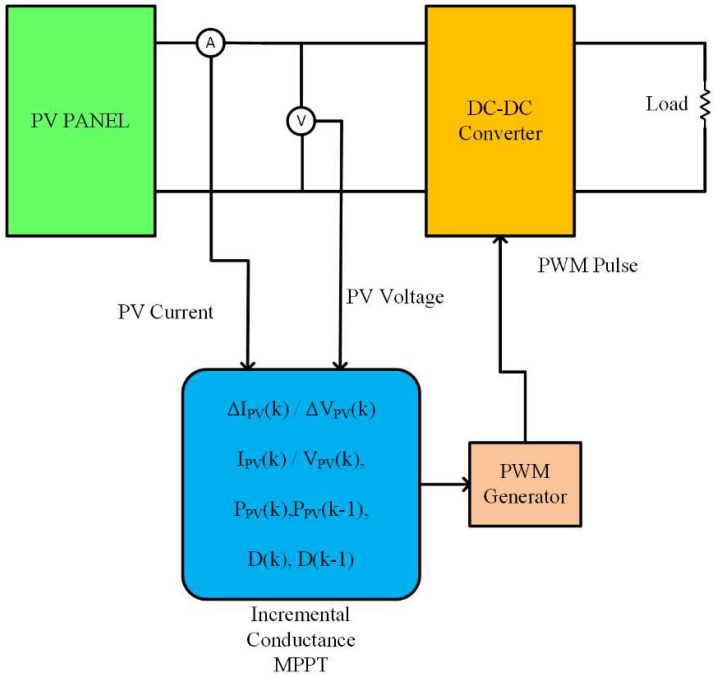

Fig 4.6: Incremental Conductance Maximum Power Point technique for Solar PV system

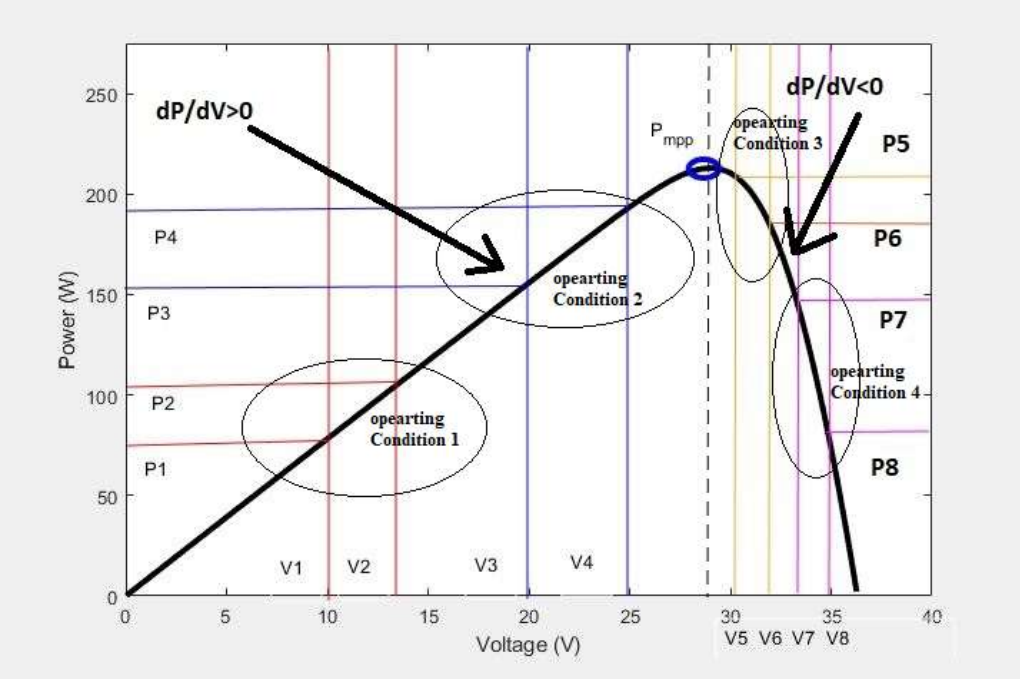

Fig 4.7: Power-Voltage characteristics of typical PV Panel

PV voltage and current are measured using a voltage and current sensor in this manner. After that voltage and current is delayed by the one sample to get the previous

sample value for PV voltage and Current. The current change is determined using the present PV current and the prior PV current. The present instant PV voltage and the previous instant PV voltage are used to determine the voltage change. The duty cycle of the incremental conductance MPPT is determined by the PV panel's incremental and instantaneous conductance. The power-voltage characteristics of the PV panel are used to show how the incremental conductance MPPT works.

Figure 5.8 depicts the power-voltage characteristics of the typical PV panel. There are four operating conditions are considered for explain the incremental conductance MPPT algorithm and it is indicated in different color such as first operating point indicated in red, second operating point indicated in blue, third operating point indicated in brown and fourth operating point indicated in pink in the Figure 5.8. Consider the first operational point, where the PV voltage is changed from V1 to V2 and the PV panel's power is changed from P1 to P2. During these conditions, the sign of change in power (P2-P1) is positive, as is the sign of change in voltage (V2-V1), and the slope of power-voltage characteristics is positive. PV voltage should be increased from V2 to some other number during these situations to move the power point closer to the PV panel's maximum power point.

$$\begin{gathered} if\ (\frac{\Delta P}{\Delta V} > 0) \\ \{V_{PV} = V2 + \Delta V\} \end{gathered} \tag{4.8}$$

Consider second operating point, PV voltage is change from V4 to V3 and PV power of the change from P4 to P3. During these conditions, the sign of the change in power (P3-P4) is negative, as is the sign of the change in voltage (V3-V4), and the slope of the power-voltage characteristics is positive. PV voltage should be increased from V3 to some other number in order to advance the power point closer to the PV panel's maximum power point.

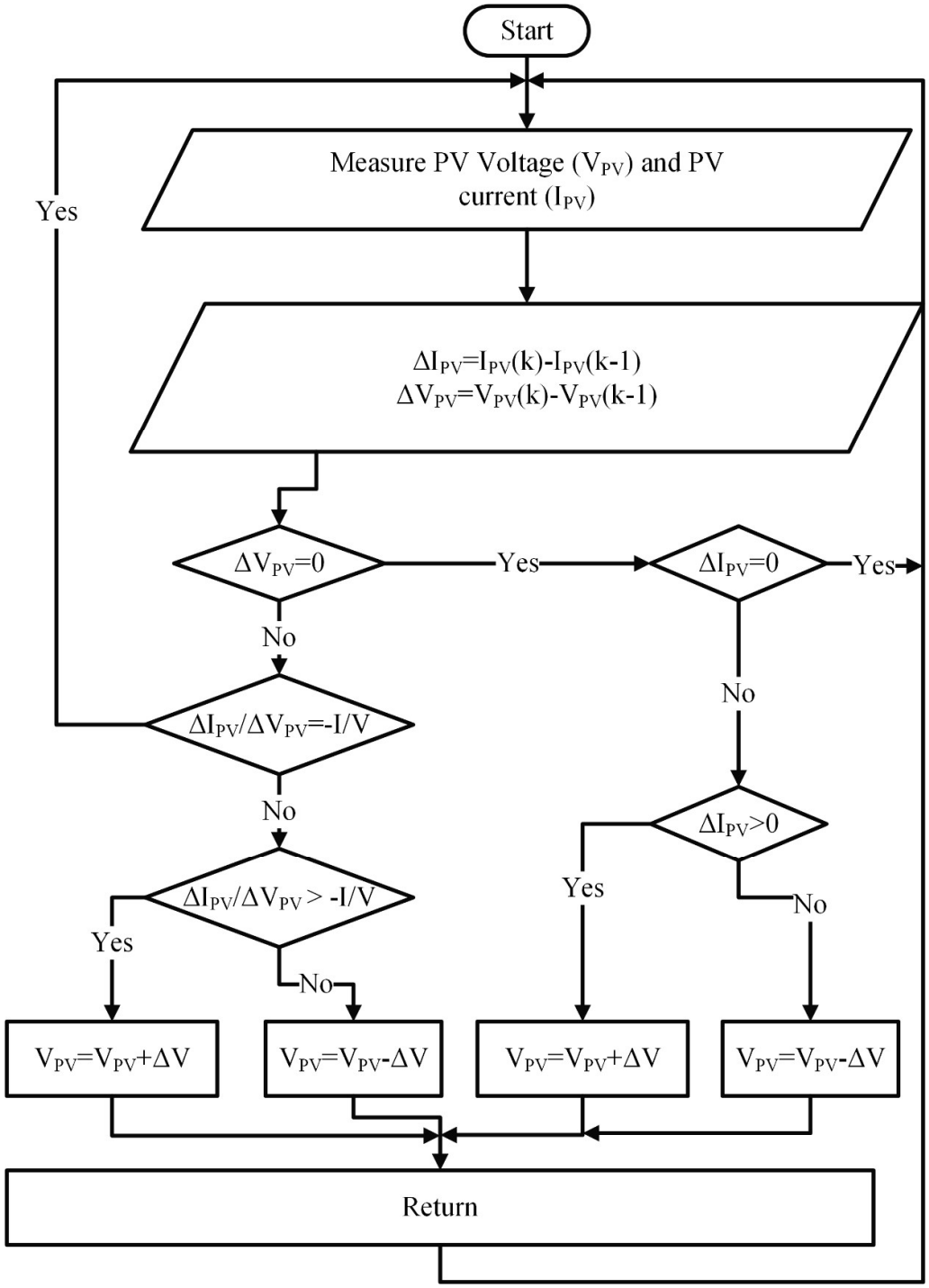

Fig 4.8: Flow Chart for Incremental Conductance MPPT.

$$if\ (\frac{\Delta P}{\Delta V} > 0) \\ \{V_{PV} = V3 + \Delta V\} \tag{4.9}$$

Consider third operating point, PV voltage is change from V5 to V6 and PV power is change from P5 to P6. During these conditions, the sign of the change in power

(P6-P5) is negative, the sign of the change in voltage (V6-V5) is positive, and the slope of the power-voltage characteristics is negative. To move the power point closer to the PV panel's MPP, the PV voltage should be reduced from V6 to some other number.

$$\begin{gathered} if\ (\frac{\Delta P}{\Delta V} < 0) \\ \{V_{PV} = V6 - \Delta V\} \end{gathered} \tag{4.10}$$

Consider fourth operating point, PV voltage is change from V8 to V7 and PV power of the change from P8 to P7. During these conditions, the sign of the change in power (P7-P8) is positive, whereas the sign of the change in voltage (V7-V8) is negative, and the slope of the power-voltage characteristics is negative. To move the power point closer to the PV panel's MPP, the PV voltage should be reduced from V7 to any other number.

$$\begin{gathered} if\ (\frac{\Delta P}{\Delta V} < 0) \\ \{V_{PV} = V7 - \Delta V\} \end{gathered} \tag{4.11}$$

Let consider $\frac{\Delta P}{\Delta V}$ is the slope of the power-voltage characteristics of the PV panel and it is rewritten as,

$$\frac{\Delta P}{\Delta V} = I + V\frac{\Delta I}{\Delta V} \tag{4.12}$$

When the PV panel reaches its maximum point and the slope of the power-voltage characteristics equals zero, it is stated as,

$$0 = I + V\frac{\Delta I}{\Delta V} \tag{4.13}$$

$$-\frac{I}{V} = \frac{\Delta I}{\Delta V} \tag{4.14}$$

Where, $\frac{\Delta I}{\Delta V}$ is the PV panel's incremental conductance, $\frac{I}{V}$ is the instantaneous conductance of the PV panel. Both will equal opposite during maximum power point conditions. when, $\frac{\Delta I}{\Delta V} > -\frac{I}{V}$, power point is lie on the left-hand side of the power-voltage characteristics , PV voltage should be increased to a certain amount to bring the power point closer to the maximum point position. When the power point is on the right-hand side of the power-voltage characteristics, PV voltage should fall to a certain value to move the power point towards the maximum point position($\frac{\Delta I}{\Delta V} < -\frac{I}{V}$). Figure 4.9 illustrates the process of the incremental conductance MPPT algorithm based on these operating

conditions. The problem with this method is that V power oscillates around the PV panel's MPP, and tracking the maximum power point takes a long time.

4.5 Fuzzy Based Maximum Power Point algorithm

To extract the maximum power from the PV array, a fuzzy-based MPPT method was applied. The fuzzy MPPT method is described by the following equation, which receives two inputs: power slope error and rate change of power slope error.

$$E_N(k) = \frac{\Delta P_N(k)}{\Delta V_N(k)} \tag{4.15}$$

$$\Delta V_N(k) = V_{pvN}(k) - V_{pvN}(k-1) \tag{4.16}$$

$$\Delta P_N(k) = P_{pvN}(k) - P_{pvN}(k-1) \tag{4.17}$$

$$\Delta E_N(k) = E_N(k) - E_N(k-1) \tag{4.18}$$

Where, $E_N(k)$ is the power slope error, $\Delta E_N(k)$ is the rate change of power slope error, $V_{pvN}(k)$ is current instant voltage of the PV array, $V_{pvN}(k-1)$ is previous instant voltage of the PV array, $P_{pvN}(k)$ is the current instant PV array power, $P_{pvN}(k-1)$ is the previous instant PV array power, $E_N(k)$ is the current instant power slope error and $E_N(k-1)$ is the previous instant power slope error.

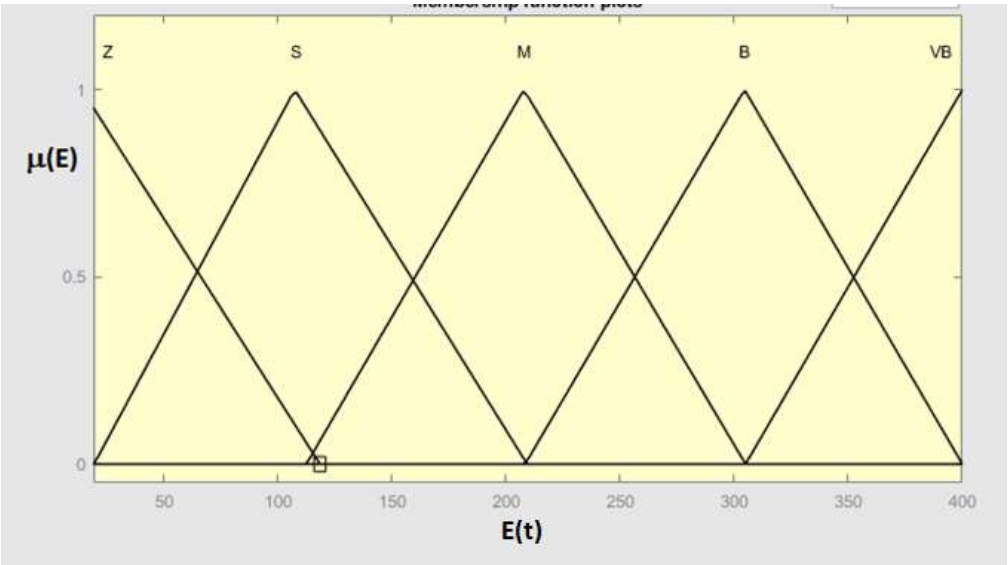

Fig 4.9: Membership function for Error

Fuzzy MPPT generates the voltage at maximum power point for the following stage based on this power slope error and rate of change of power slope error. Figures 4.9 and 4.10 demonstrate the membership function for power slope error and rate of change of power slope error, respectively.

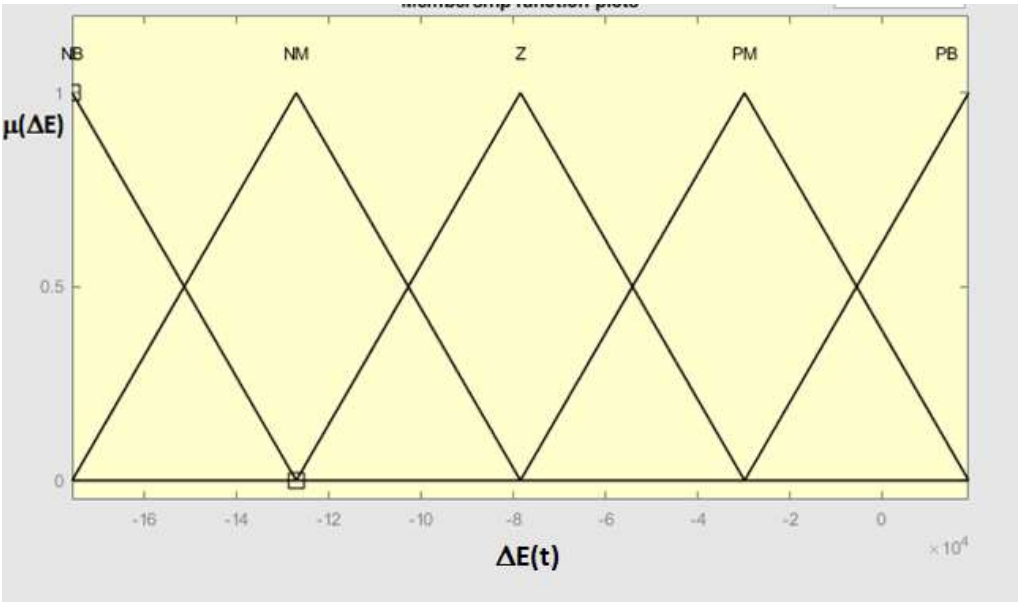

Fig 4.10 Membership function for rate of change of Error.

Table 4.1. Rule base for MPPT algorithm

$E_N(k)$ / $\Delta E_N(k)$	**NB**	**NM**	**Z**	**PM**	**PB**
Z	0	0	56	67	0
S	0	0	179	60	0
M	0	0	92	77	60
B	85	57	72	69	76
VB	55	82	143	73	72

The Fuzzy based MPPT is modeled using sugeno fuzzy inference system. The membership functions for error and rate of change of error are Zero (Z), Small (S), Big (B), Very Big (VB), Negative Big (NB), Negative Medium (NM), Positive Medium (PM), and Positive Big (PB). Total twenty-five rule has been created in the fuzzy inference system for implementing MPPT algorithm and rule structure is shown in Table 4.1.

4.6. Conclusion

Different MPPT techniques for the PV system are covered in this chapter, including both conventional and intelligent control strategies. The traditional techniques of P&O and InC, as well as the intelligent control technique of fuzzy logic controller, are explored.

CHAPTER 5

Simulink Model Of Grid Connected PV System

5.1. GENERAL

The output power of a PV cell in a solar PV system is determined by environmental factors such as temperature and sun irradiation. Because the maximum power point varies depending on the irradiance value, tracking the maximum power point is required for optimal output. Researchers have already devised and executed a variety of maximum power point techniques. The techniques of incremental conductance and fuzzy MPPT are researched and implemented in MATLAB/Simulink in this chapter.

5.2. Simulink model of the proposed system

The overall Simulink model of the proposed system is depicted in Figure 5.1. The control algorithm for the MPPT control and grid control is illustrated in Figure 5.2.

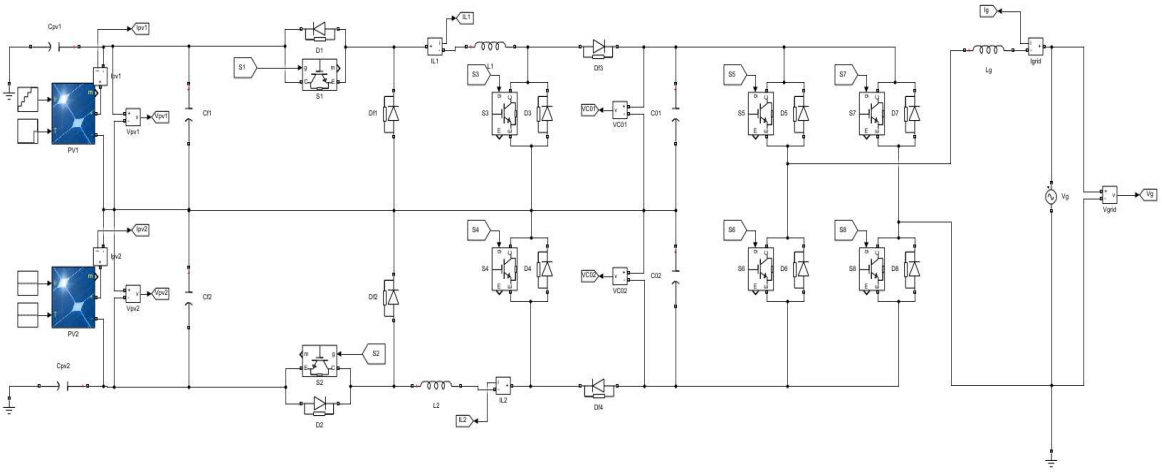

Fig 5.1: The overall Simulink model of the solar PV integrated with grid system.

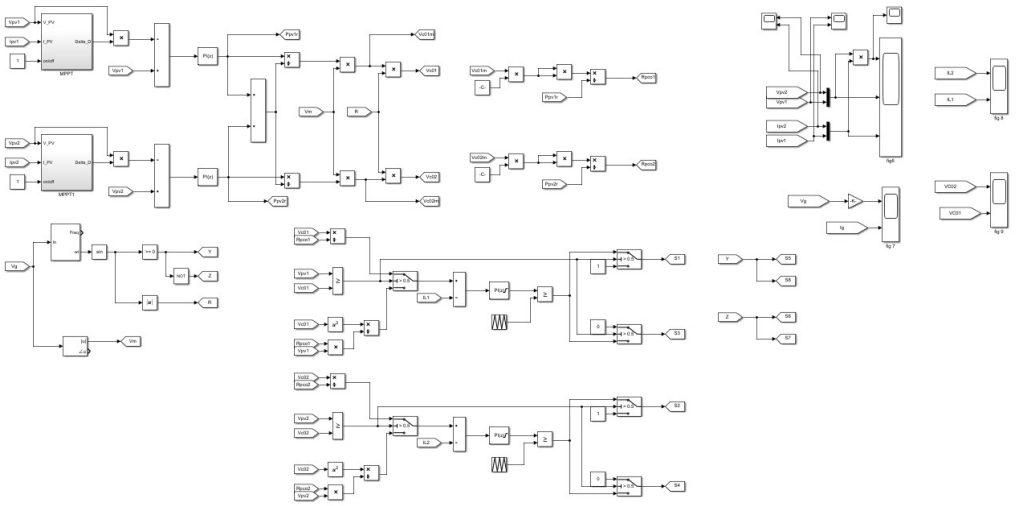

Fig 5.2: The control algorithm for the proposed system.

Figure 5.3 illustrates the Simulink model of the incremental conductance MPPT. PV voltage and current are used as inputs for the incremental conductance MPPT, and the output is the voltage at the PV panel's maximum power point.

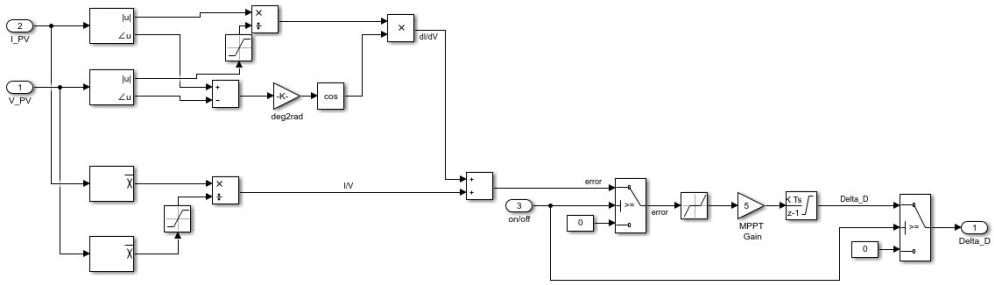

Fig 5.3: Simulink model of incremental conductance MPPT.

The fuzzy MPPT's Simulink model is depicted in Figure 5.4. The fuzzy MPPT's inputs include PV voltage and current. The delay of the PV voltage and current is used to calculate the change voltage and current, which is then compared to the current instant PV voltage and current. The error and rate of change of error are determined and provided to the fuzzy logic controller using change voltage and current. The voltage at the PV panel's highest power point is the output of the fuzzy logic controller.

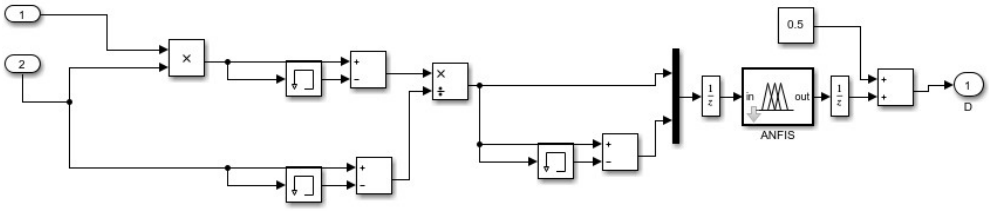

Fig 5.4: Simulink model of Fuzzy MPPT.

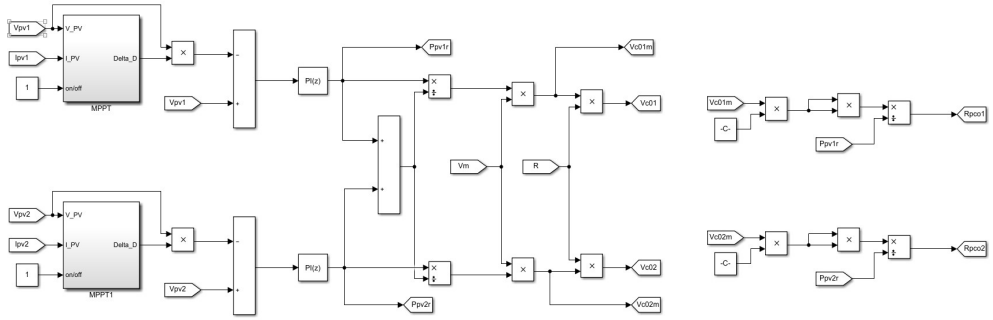

Fig 5.5: Simulink model for generation of Vco1, Vco2, Rpco1 and Rpco2.

The Simulink model for generation of Vco1, Vco2, Rpco1 and Rpco2 is shown in the Figure 5.5. Two different MPP trackers and two proportional integral (PI) controllers are utilized to calculate the values of Ppv1 and Ppv2, which are required to estimate Vco1m and Vco2m. Vco1m and Vco2m are calculated using Vm's phase locked loop information (PLL). The mode of operation of CONV1 (buck or boost) is identified by comparing Vpv1 and Vco1, whereas the mode of operation of CONV2 is determined by comparing Vpv2 and Vco2. The two component converters' emulated effective resistances, Rpco1 and Rpco2, are calculated by estimating the RMS values of Vco1 and Vco2, which are then squared and divided by Ppv1 and Ppv2.These signals are used for generating reference current for grid integration.

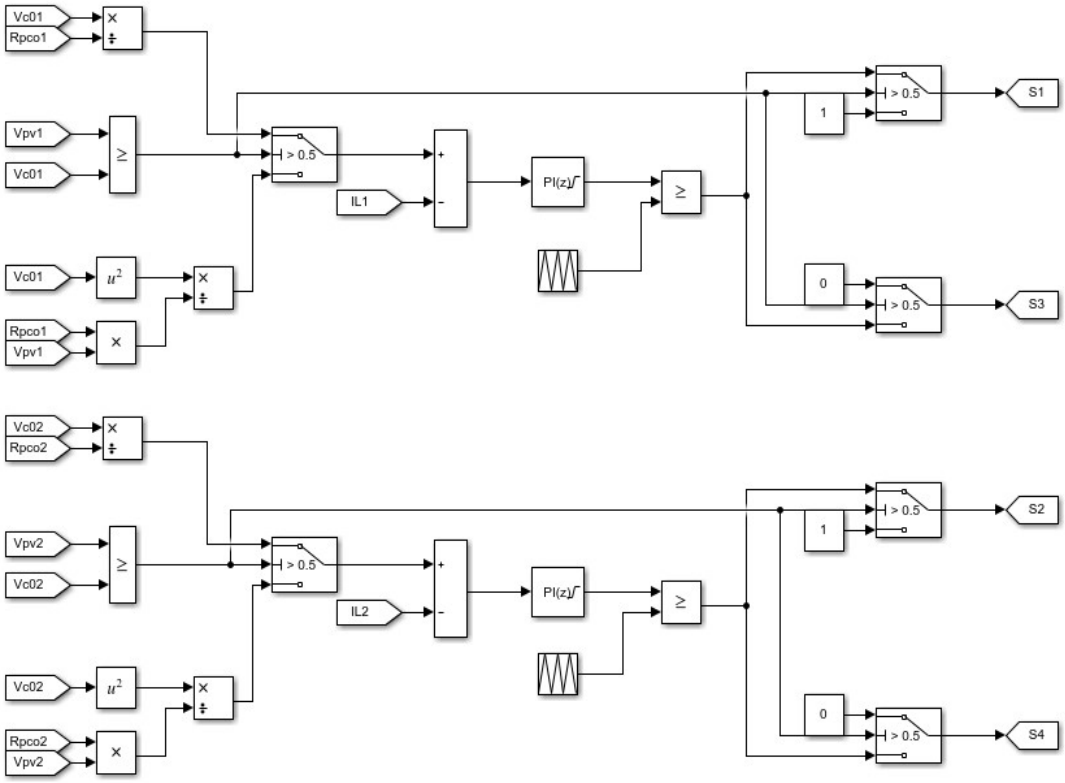

Fig 5.6: Pulse generation logic for dual buck boost DC-DC converter.

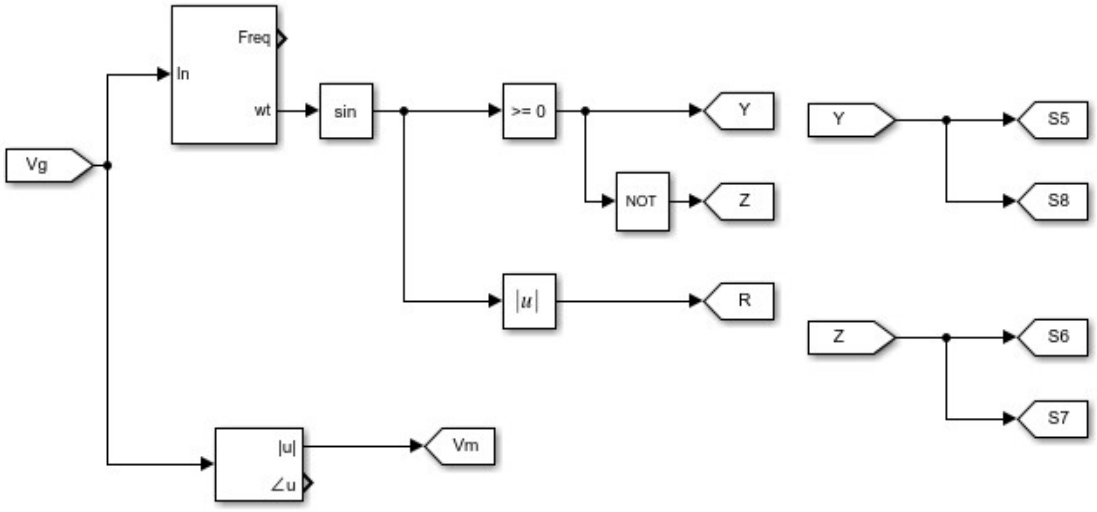

Fig 5.7: Pulse generation logic for single phase grid tied inverter.

The Simulink model for pulse generation of the dual buck boost converter is depicted in Figure 5.6. Current reference command is generated based on the Vpv, Vco1, Vco2, Rpco1 and Rpco2. The current reference command is compared with inductor currents and processed via PI controller. To generate the pulse for the dual buck boost converter, the PI controller output is compared to the carrier wave. Figure 5.7 depicts the pulse generating logic for a single phase grid linked inverter. In next section simulation of the proposed system with constant irradiance, varying irradiance, constant temperature and varying temperature is discussed. The simulation results of the following cases are discussed in the subsequent section and details are presented in the Table 5.1.

Table 5.1. Test Case

Case	PV1 Irradaince (W/m2)	PV1 Temperature (°C)	PV2 Irradaince (W/m2)	PV2 Temperature (°C)
1	500	25	800	25
2	700	25	800	25
3	1000	25	800	25

5.3. Simulink results of the proposed system with Case1

The proposed system is tested under the following operating conditions: the PV array 1's irradiance and temperature are set at 500 W/m2 and 25°C, while the PV array 2's irradiance and temperature are set at 800 W/m2 and 25°C.

Figure 5.8 depicts the PV power, voltage, current, Grid voltage and current with incremental conductance MPPT.

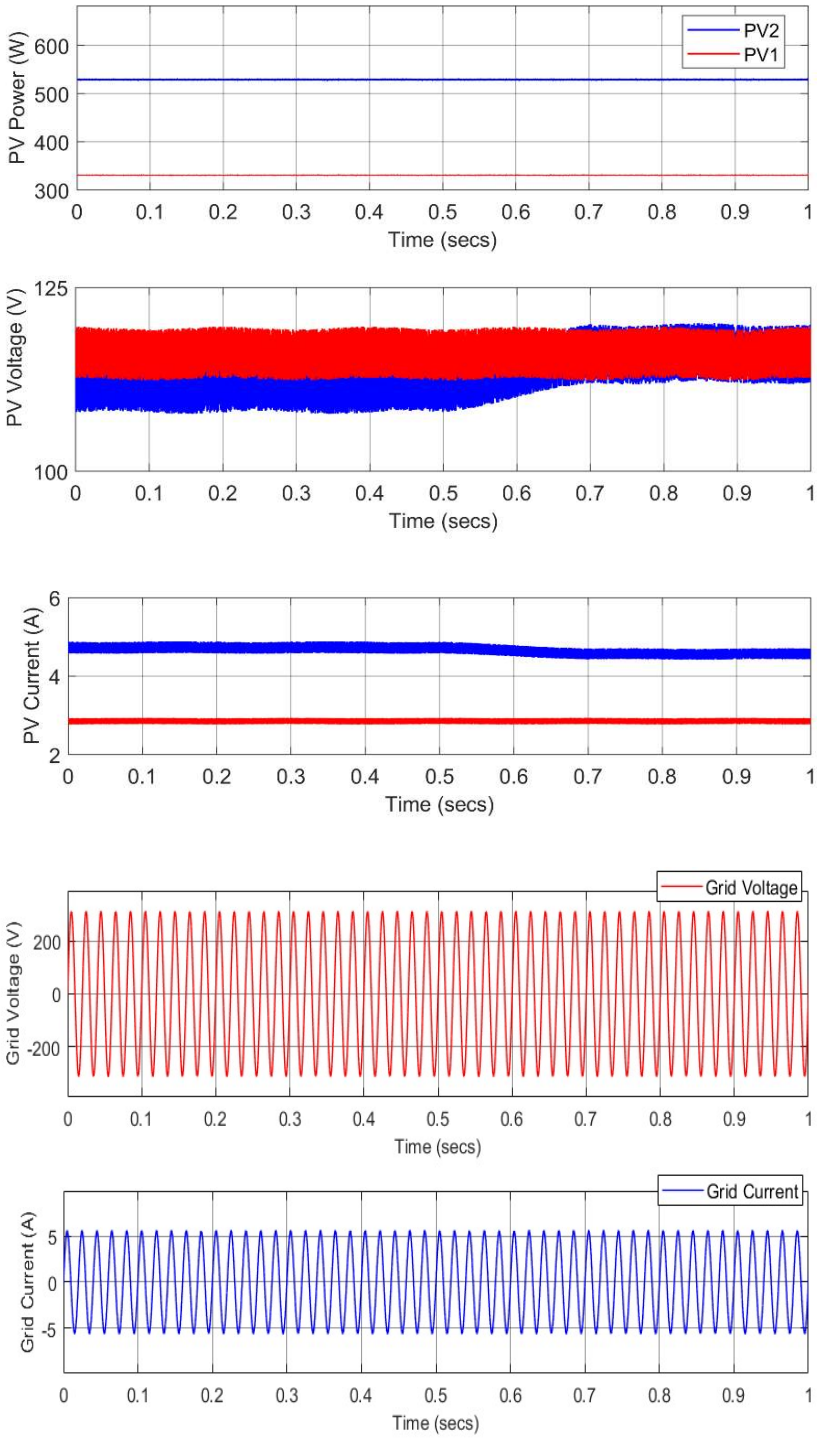

Fig 5.8: PV Power, Voltage, Current of the PV array 1 & 2; Grid Voltage and Current with Incremental Conductance MPPT for Case1.

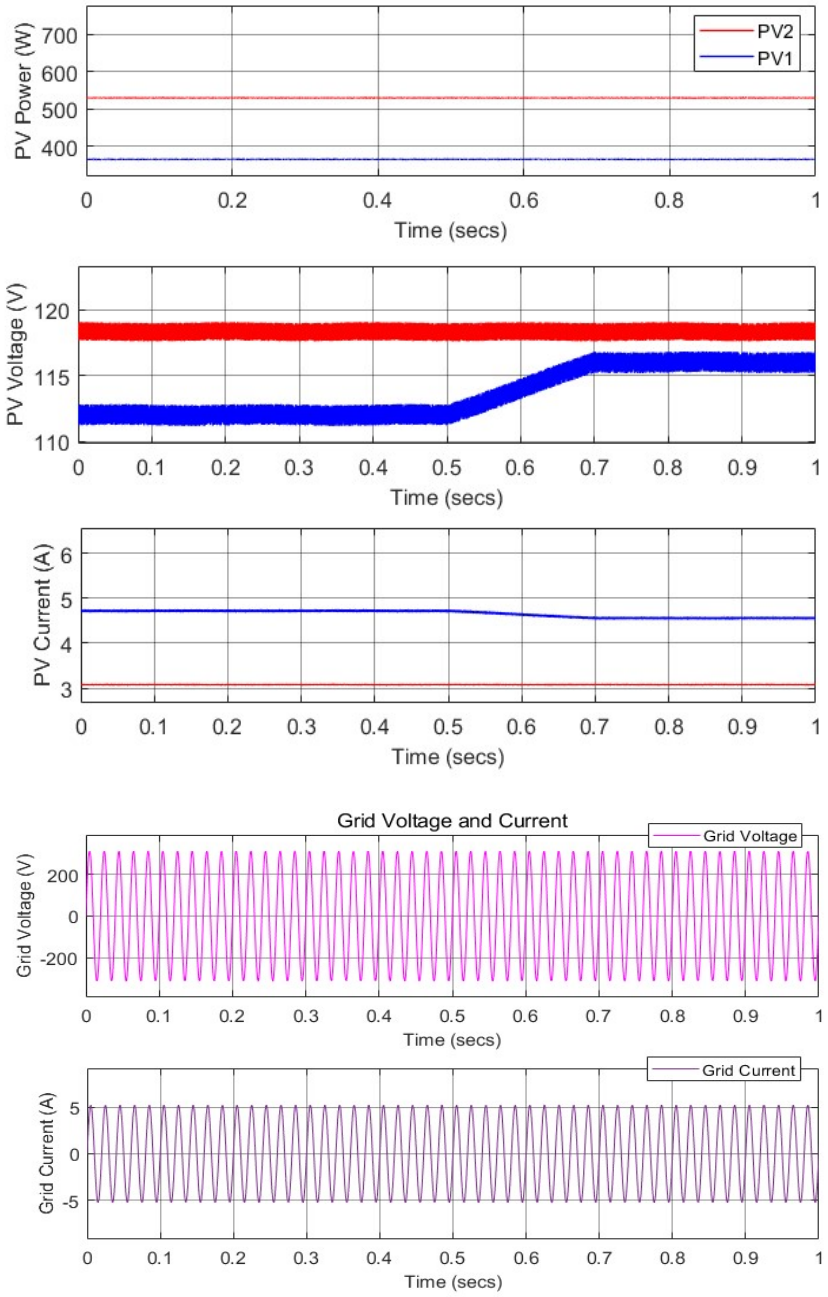

Fig 5.9: PV Power, Voltage, Current of the PV array 1 & 2; Grid Voltage and Current with Fuzzy MPPT for Case1.

In this condition, PV array 1 & 2 power are 330 W & 530W, PV array's 1 & 2 voltage is around 115 V & 112 V, PV array's 1 & 2 current are around 2.86 A & 4.73 A and grid is around 3.73 A with incremental conductance MPPT. PV array 1 & 2 power are 350 W & 540 W, PV array's 1 & 2 voltage is around 118 V & 113 V, PV array's 1 & 2 current are around 2.96 A & 4.77 A and grid is around 3.86 A with fuzzy MPPT.

5.4. Simulink results of the proposed system with Case2

The proposed system is tested under the following operating conditions: the PV array 1's irradiance and temperature are set at 700 W/m2 and 25°C, while the PV array 2's irradiance and temperature are set at 800 W/m2 and 25°C.

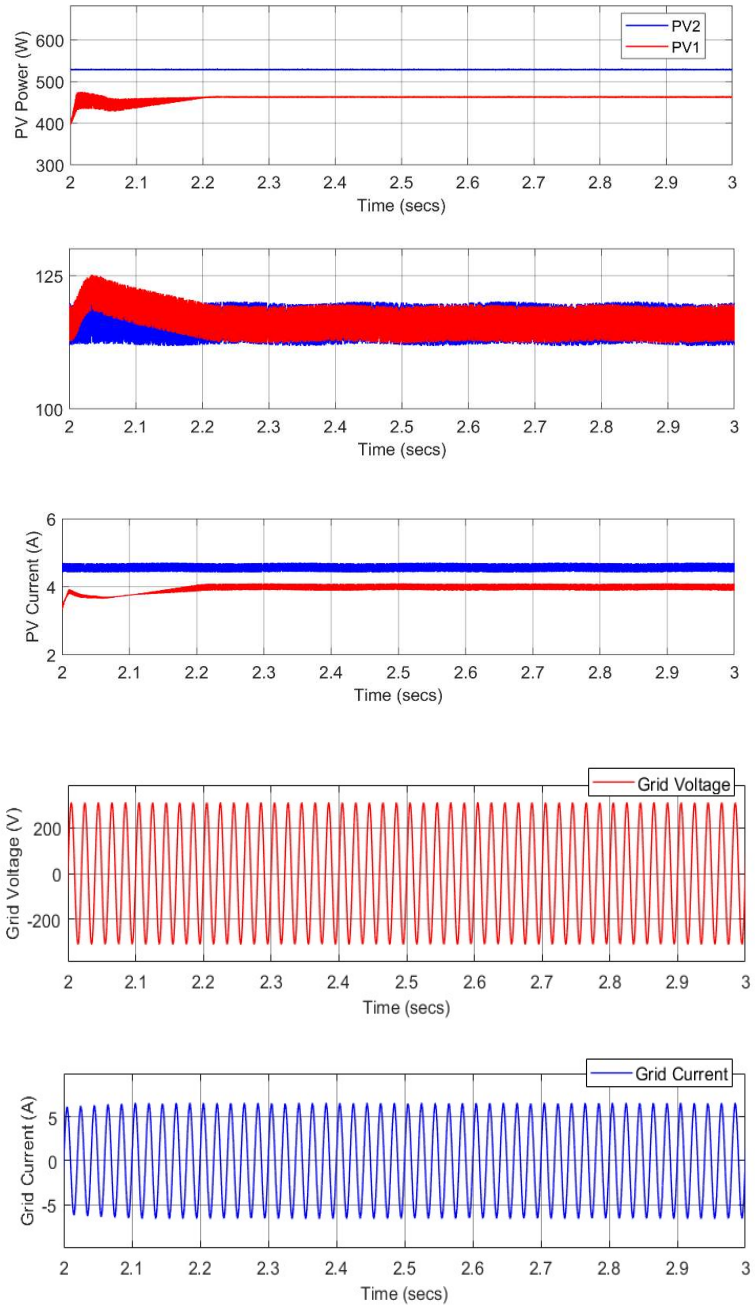

Fig 5.10: PV Power, Voltage, Current of the PV array 1 & 2; Grid Voltage and Current with Incremental Conductance MPPT for Case2.

Figure 5.10 depicts the PV power, voltage, current, Grid voltage and current with incremental conductance MPPT. Figure 5.11 depicts the PV power, voltage, current, Grid voltage and current with fuzzy MPPT.

In this condition, PV array 1 & 2 power are 480 W & 530W, PV array's 1 & 2 voltage is around 115 V & 115 V, PV array's 1 & 2 current are around 4.17 A & 4.6 A and grid is around 4.39 A with incremental conductance MPPT. PV array 1 & 2 power are 510 W & 540 W, PV array's 1 & 2 voltage is around 118 V & 116 V, PV array's 1 & 2 current are around 4.32 A & 4.65 A and grid is around 4.56 A with fuzzy MPPT.

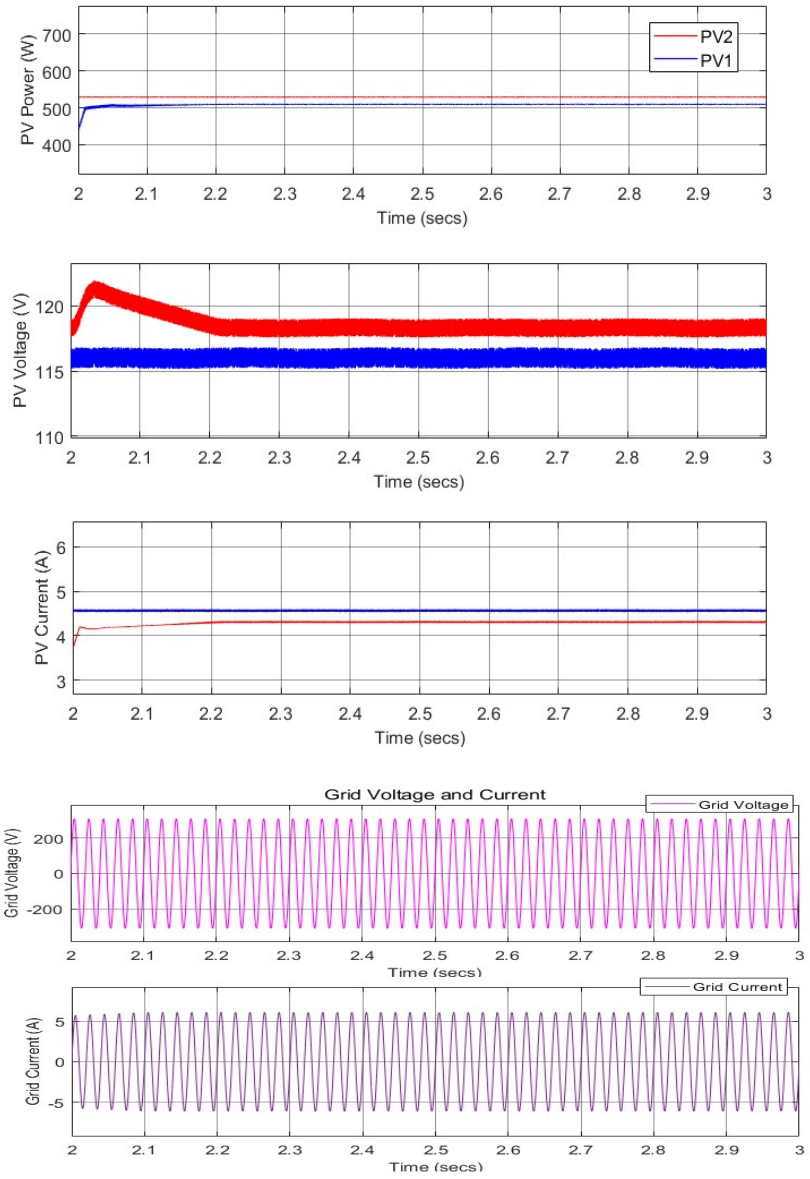

Fig 5.11: PV Power, Voltage, Current of the PV array 1 & 2; Grid Voltage and Current with Fuzzy MPPT for Case2.

5.5. Simulink results of the proposed system with Case3

The proposed system is tested under the following operating conditions: the PV array 1's irradiance and temperature are set at 1000 W/m2 and 25°C, while the PV array 2's irradiance and temperature are set at 800 W/m2 and 25°C. Figure 5.12 depicts the PV power, voltage, current, Grid voltage and current with incremental conductance MPPT. Figure 5.13 illustrates the PV power, voltage, current, Grid voltage and current with fuzzy MPPT. In this condition, PV array 1 & 2 power are 650 W & 530W, PV array's 1 & 2 voltage is around 115 V & 115 V, PV array's 1 & 2 current are around 5.65 A & 4.6 A and grid is around 5.13 A with incremental conductance MPPT. PV array 1 & 2 power are 720 W & 540 W, PV array's 1 & 2 voltage is around 118 V & 116 V, PV array's 1 & 2 current are around 6.1 A & 4.65 A and grid is around 5.47 A with fuzzy MPPT.

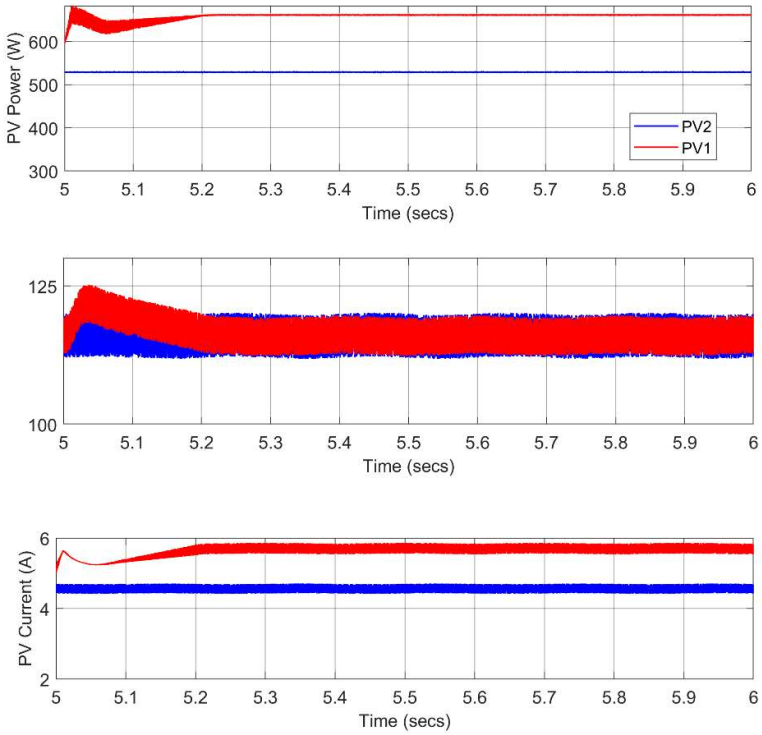

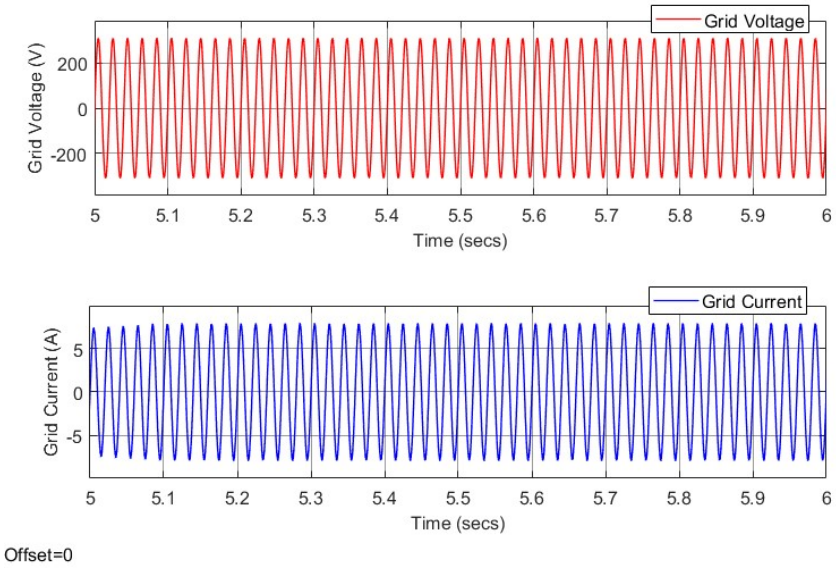

Fig 5.12: PV Power, Voltage, Current of the PV array 1 & 2; Grid Voltage and Current with Incremental conductance MPPT for Case3.

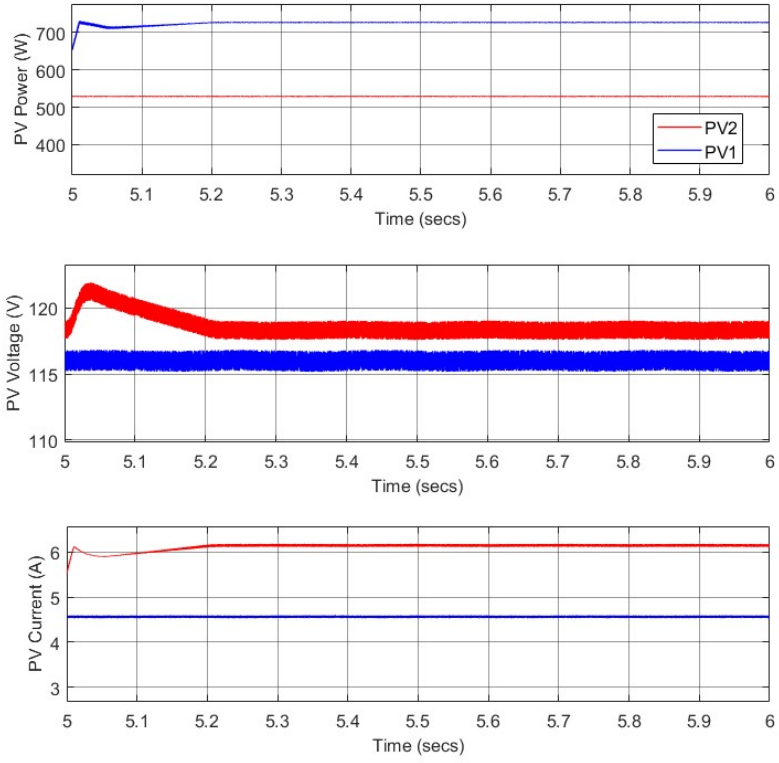

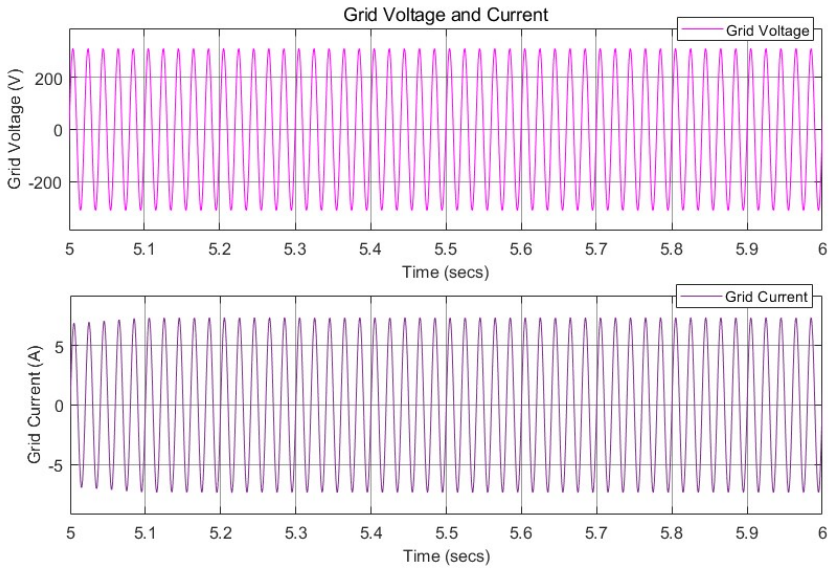

Fig 5.13: PV Power, Voltage, Current of the PV array 1 & 2; Grid Voltage and Current with Fuzzy MPPT for Case3.

5.6. Simulink results of the proposed system with varying irradiance condition

The proposed model tested with following conditions i.e., PV array 1 irradiance varied at every 1 sec at 500, 600, 700, 800, 900 & 1000 W/m^2. PV array 2 irradiance set 800 W/m^2. Figure 5.13 depicts the PV power, voltage, current grid voltage and current with incremental conductance MPPT. Figure 5.14 shows the total harmonic distortion of the grid current with incremental conductance MPPT. With incremental conductance MPPT, the PV voltage and current oscillate more, and the PV power oscillates around the maximum power point as well. With incremental conductance MPPT, total harmonic distortion of the grid current is 2.09 percent.

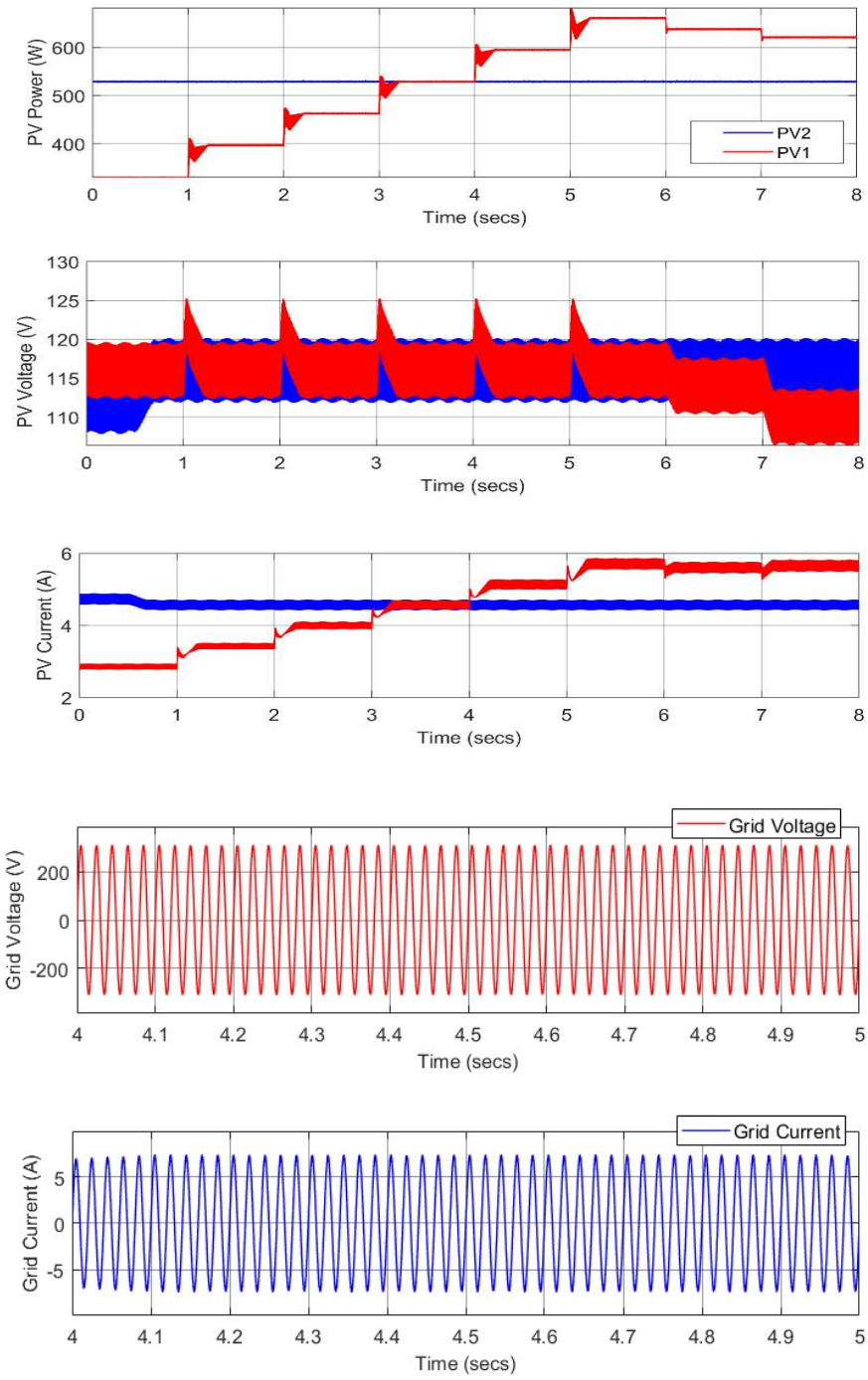

Fig 5.14: PV Power, Voltage, Current, Grid voltage and Current with Incremental Conductance MPPT for varying irradiance.

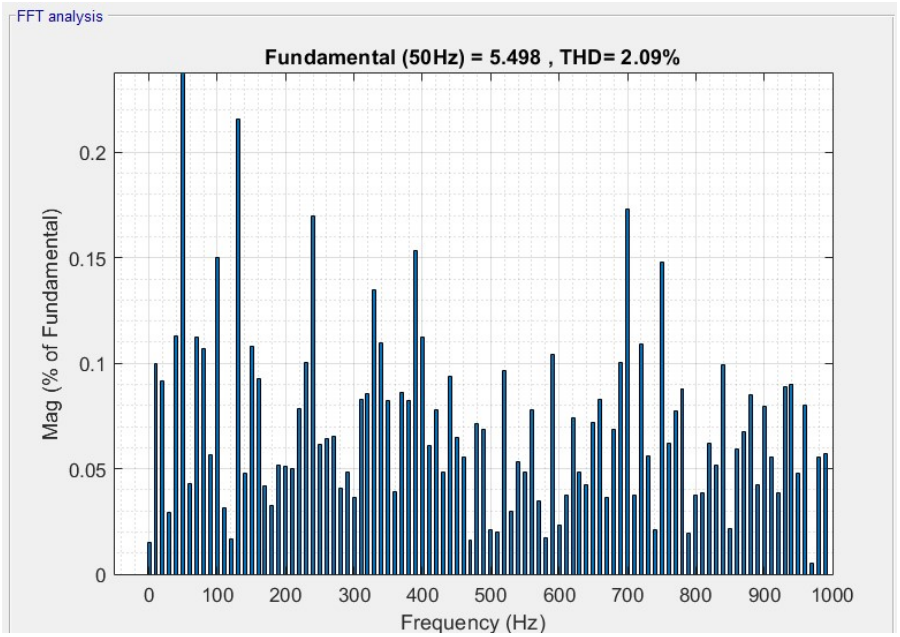

Fig 5.15: Total Harmonic Distortion of Grid Current with Incremental Conductance MPPT.

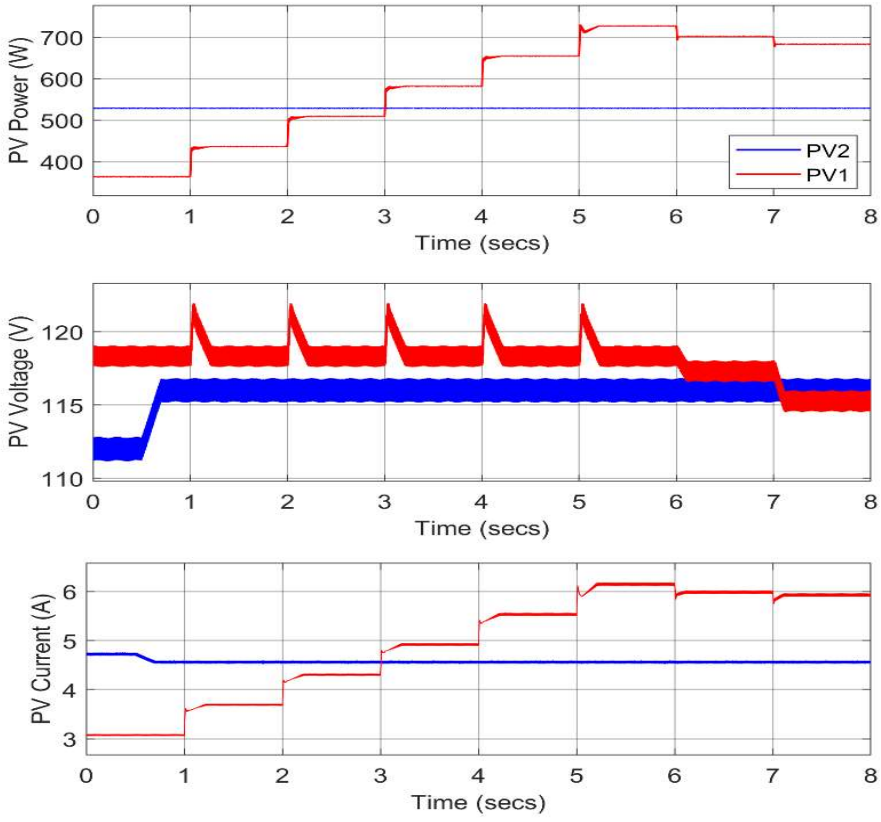

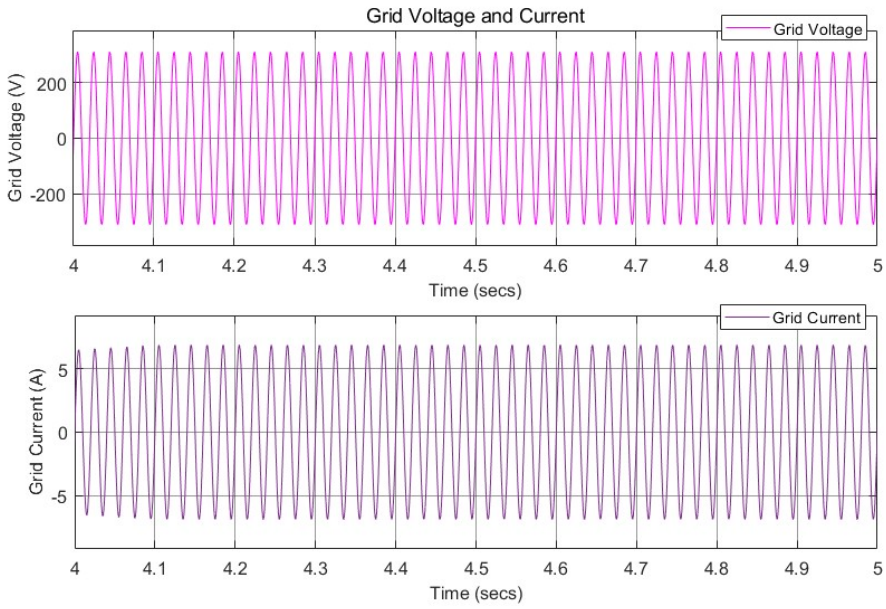

Fig 5.16: PV Power, Voltage, Current, Grid Voltage and Current with Fuzzy MPPT for varying irradiance.

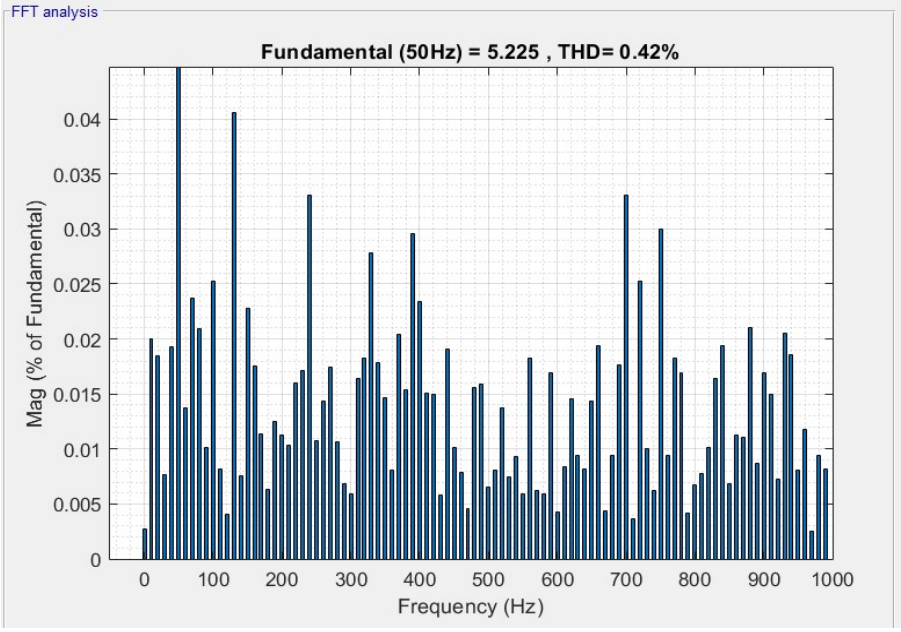

Fig 5.17: Total Harmonic Distortion of grid Current with Fuzzy MPPT

With Fuzzy MPPT, the PV power, voltage, current, grid voltage, and current are shown in Figure 5.16. The overall harmonic distortion of the grid current with fuzzy MPPT is shown in Figure 5.17. Because the maximum power is obtained rapidly, the PV voltage and current oscillate less using Fuzzy MPPT. With fuzzy MPPT, total harmonic distortion of the grid current is 0.42 %.

5.7. Comparison of Results

Table 5.2 Comparison of Fuzzy Mppt and Incremental Conductance MPPT

IRRADIANCE (W/m^2) & TEMPERATURE (25°C)	INCREMENTAL CONDUTANCE MPPT	FUZZY MPPT
	POWER (W)	
500	325.2	333.1
700	458.1	466.1
1000	650.2	660.5

Comparison of maximum power of the PV array 1 at 500,700 and 1000 W/m^2 with incremental conductance method and Fuzzy MPPT is shown in Table 5.3. From these test results, incremental conductance MPPT has maximum power extraction ratio around 97 to 98 % but Fuzzy MPPT has maximum power extraction ratio around 99.2 to 99.6 %.

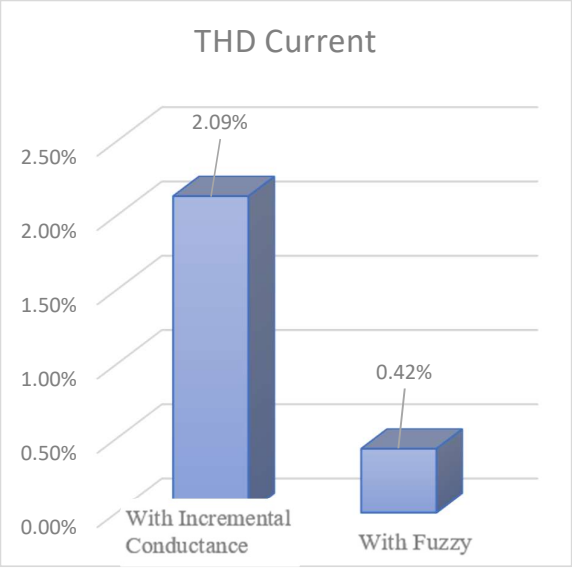

Fig 5.18: Comparison of Total harmonic Distortion of grid Current

From Figure 5.18 it is clear that Fuzzy MPPT shows improved performance of 397% compared to Incremental Conductance MPPT in case of grid current THD.

5.8. Conclusion

The proposed Simulink model and simulation results are discussed in this chapter. The proposed model was tested under several situations, including constant and variable irradiance, incremental conductance, and a fuzzy MPPT algorithm. According to the test results, fuzzy MPPT outperforms incremental conductance MPPT for the suggested system.

CHAPTER 6

Conclusion and Future Scope

6.1. Conclusion

Sugeno Type Fuzzy Logic MPPT Controller for Grid Connected PV System under Mismatched Environmental Conditions was discussed in this paper. In the MATLAB Simulink environment, the above model is developed and tested. With fuzzy MPPT and incremental conductance MPPT, the suggested system was tested for constant and variable irradiance conditions. According to the findings of the tests, fuzzy MPPT extracts 99.5 percent more maximum power from the solar PV array than incremental conductance MPPT, and it also extracts maximum power from the solar PV array faster than incremental conductance MPPT. Finally, the proven dual buck boost converter with fuzzy MPPT algorithm is a good choice for grid-connected solar PV.

6.2. Future scope

In future the work presented in thesis can be extended to:

- For the proposed system hardware implementation can be done.
- Other intelligent and adaptive control algorithms for MPPT grid connected PV system under partial shading conditions.
- Transient response of the proposed system can be improved.

References

[1] Ezhiljenekkha, G.; MarsalineBeno, M. Review of Power Quality Issues in Solar and Wind Energy. Mater. Today Proc. 2020, 24, 2137–2143.

[2] K.N. Nwaigwe, P. Mutabilwa, E. Dintwa, An overview of solar power (PV systems) integration into electricity grids, Materials Science for Energy Technologies, Volume 2, Issue 3, 2019, Pages 629-633.

[3] Li, W.; Ren, H.; Chen, P.; Wang, Y.; Qi, H. Key Operational Issues on the Integration of Large-Scale Solar Power Generation—A Literature Review. Energies 2020, 13, 5951.

[4] Seme, S.; Štumberger, B.; Hadžiselimovi´c, M.; Sredenšek, K. Solar Photovoltaic Tracking Systems for Electricity Generation: A Review. Energies 2020, 13, 4224.

[5] Eltawil, M.A.; Zhao, Z. Grid-connected photovoltaic power systems: Technical and potential problems—A review. Renew. Sustain. Energy Rev. 2010, 14, 112–129.

[6] Islam, M.; Nadarajah, M.; Hossain, M.J. A Grid-Support Strategy with PV Units to Boost Short-Term Voltage Stability Under Asymmetrical Faults. IEEE Trans. Power Syst. 2020, 35, 1120–1131.

[7] Eltawil, M.A.; Zhao, Z. Grid-connected photovoltaic power systems: Technical and potential problems—A review. Renew. Sustain. Energy Rev. 2010, 14, 112–129.

[8] Zhang, W.; Zhou, G.; Ni, H.; Sun, Y. A Modified Hybrid Maximum Power Point Tracking Method for Photovoltaic Arrays Under Partially Shading Condition. IEEE Access 2019, 7, 160091–160100.

[9] Samara, S.; Natsheh, E. Intelligent Real-Time Photovoltaic Panel Monitoring System Using Artificial Neural Networks. IEEE Access 2019, 7, 50287–50299.

[10] Ali, A.; Almutairi, K.; Malik, M.Z.; Irshad, K.; Tirth, V.; Algarni, S.; Zahir, M.; Islam, S.; Shafiullah, M.; Shukla, N.K. Review of online and soft computing maximum power point tracking techniques under non-uniform solar irradiation conditions. Energies 2020, 13, 3256.

[11] Abdouramani Dadjé, Noël Djongyang, Janvier Domra Kana & Réné Tchinda 2016, 'Maximum power point tracking methods for photovoltaic systems operating under partially shaded or rapidly variable insolation conditions: a review paper', International Journal of Sustainable Engineering, vol. 9, no. 4, pp. 224-239.

[12] Alice Hepzibah, A & Premkumar, K 2020, 'ANFIS current–voltage controlled MPPT algorithm for solar powered brushless DC motor based water pump', Electrical Engineering, vol.102, pp. 421-435.

[13] Anup Anurag, Satarupa Bal, Suman Sourav & Mrutyunjaya Nanda 2016, 'A review of maximum power- point tracking techniques for photovoltaic systems', International Journal of Sustainable Energy, vol. 35. no. 5, pp. 478-501.

[14] Bahrami, M, Gavagsaz-Ghoachani, R, Zandi, M, Phattanasak, M, Maranzanaa, G, Nahid-Mobarakeh, B, Pierfederici, S & Meibody-Tabar, F 2019, 'Hybrid maximum power point tracking algorithm with improved dynamic performance', Renewable energy, vol.130,
pp. 982-991.

[15] Bataineh, K 2018, 'Improved hybrid algorithms-based MPPT algorithm for PV system operating under severe weather conditions', IET Power Electronics, vol. 12, no. 4, pp.703-711.

[16] Belhachat, F & Larbes, C 2017, 'Global maximum power point tracking based on ANFIS approach for PV array configurations under partial shading conditions', Renewable and Sustainable Energy Reviews, vol. 77, pp. 875-889.

[17] Boumaaraf, H, Talha, A & Bouhali, O 2015, 'A three-phase NPC grid-connected inverter for photovoltaic applications using neural network MPPT', Renewable and Sustainable Energy Reviews, vol.49, pp. 1171-1179.

[18] Da Luz, CMA, Vicente, EM & Tofoli, FL 2020, 'Experimental evaluation of global maximum power point techniques under partial shading conditions', Solar Energy, vol. 196, pp. 49-73.

[19] Danandeh, MA 2018, 'A new architecture of INC-fuzzy hybrid method for tracking maximum power point in PV cells', Solar Energy, vol. 171, pp. 692-703.

[20] Faiza Belhachat & Cherif Larbes 2017, 'Global maximum power point tracking based on ANFIS approach for PV array configurations under partial shading conditions', Renewable and Sustainable Energy Reviews, vol. 77, pp. 875-889.

[21] Fernando Lessa Tofoli, Dênis de Castro Pereira & Wesley Josias de Paula 2015, 'Comparative Study of Maximum Power Point Tracking Techniques for Photovoltaic Systems', International Journal of Photoenergy, vol. 2015, Article ID 812582, pp. 1-10.

[22] Gosumbonggot, Jirada & Goro Fujita 2019, 'Partial shading detection and global maximum power point tracking algorithm for photovoltaic with the variation of irradiation and temperature', Energies, vol.12, no. 202, pp. 1-22.

[23] Houria Boumaaraf, Abdelaziz Talha & Omar Bouhali 2015, 'A three-phase NPC grid-connected inverter for photovoltaic applications using neural network MPPT', Renewable and Sustainable Energy Reviews, vol. 49, pp. 1171-1179.

[24] Hsu, TW, Wu, HH, Tsai, DL & Wei, CL 2018, 'Photovoltaic energy harvester with fractional open-circuit voltage based maximum power point tracking circuit', IEEE Transactions on Circuits and Systems II: Express Briefs, vol. 66, no. 2, pp. 257-261.

[25] Hu, K, Cao, S, Li, W & Zhu, F 2019, 'An Improved Particle Swarm Optimization Algorithm Suitable for Photovoltaic Power Tracking under Partial Shading Conditions', IEEE Access, vol.7, pp.143217-143232.

[26] Jirada Gosumbonggot 2016, 'Maximum Power Point Tracking Method using Perturb and Observe Algorithm for Small Scale DC Voltage Converter', Procedia Computer Science, vol. 86, pp. 421-424.

[27] Kante Visweswara 2014, 'An Investigation of Incremental Conductance based Maximum Power Point Tracking for Photovoltaic System', Energy Procedia, vol. 54, pp.11-20.

[28] Khanaki, Razieh, Mohd Radzi, Mohd Amran & Marhaban, Mohammad Hamiruce 2014, 'Artificial neural network based maximum power point tracking controller for photovoltaic standalone system', International Journal of Green Energy, vol.13, no.3, pp. 1543-5075.

[29] Kumar, R, Khandelwal, S, Upadhyay, P & Pulipaka, S 2019, 'Global maximum power point tracking using variable sampling time and pv curve region shifting technique along with incremental conductance for partially shaded photovoltaic systems', Solar Energy, vol.189, pp.151-178.

[30] Li, G, Jin, Y, Akram, MW, Chen, X & Ji, J 2018, 'Application of bio-inspired algorithms in maximum power point tracking for PV systems under partial shading conditions–A review', Renewable and Sustainable Energy Reviews, vol. 81, pp.840-873.

[31] Li, W, Zhang, G, Pan, T, Zhang, Z, Geng, Y & Wang, J 2019, A Lipschitz Optimization-Based MPPT Algorithm for Photovoltaic System Under Partial Shading Condition. IEEE Access, vol.7, pp.126323-126333.

[32] Lyden, S & Haque, ME 2015, 'Maximum Power Point Tracking techniques for photovoltaic systems: A comprehensive review and comparative analysis', Renewable and Sustainable Energy Reviews, vol. 52, pp. 1504-1518.

[33] Mehmet Sait Cengiz & Mehmet Salih Mamiş 2015, 'Price-Efficiency Relationship for Photovoltaic Systems on a Global Basis', International Journal of Photoenergy, vol.2015, Article ID 256101, pp. 1-12.

[34] Mehreen Gul, Yash Kotak & Tariq Muneer 2016, 'Review on recent trend of solar photovoltaic technology', Energy Exploration & Exploitation, vol. 34, no. 4, pp. 485-526.

[35] Mostafa, MR, Saad, NH & El-sattar, AA 2020, 'Tracking the maximum power point of PV array by sliding mode control method', Ain Shams Engineering Journal, vol. 11, no. 1, pp. 119-131.

[36] Nabipour, M, Razaz, M, Seifossadat, SGH & Mortazavi, SS 2017, 'A new MPPT scheme based on a novel fuzzy approach', Renewable and Sustainable Energy Reviews, vol. 74, pp. 1147-1169.

[37] Padmanaban, S, Priyadarshi, N, Bhaskar, MS, Holm-Nielsen, JB, Ramachandaramurthy, VK & Hossain, E 2019, 'A Hybrid ANFIS-ABC Based MPPT Controller for PV System With Anti-Islanding Grid Protection: Experimental Realization', IEEE Access, vol.7, pp.103377-103389.

[38] Premkumar, K & Manikandan, BV 2018, 'Stability and Performance Analysis of ANFIS Tuned PID Based Speed Controller for Brushless DC Motor', Current Signal Transduction Therapy, vol.13, no.1, pp. 19-30.

[39] Premkumar, K & Manikandan, BV 2014, 'Adaptive Neuro Fuzzy Inference System based speed controller for brushless DC motor', Neurocomputing, vol.138, pp. 260-270.

[40] Putri, RI, Pujiantara, M, Priyadi, A, Ise, T & Purnomo, MH 2017, 'Maximum power extraction improvement using sensorless controller based on adaptive perturb and observe algorithm for PMSG wind turbine application', IET Electric Power Applications, vol.12, no.4, pp.455-462.

[41] Rathi, KJ & Ali, MS 2016, 'NFC Design using ANFIS for Power Electronics Circuits', International Journal of Innovative Research In Electrical, Electronics, Instrumentation and Control Engineering, vol.4, no. 3, pp. 9-12.

[42] RatnaIka Putri, Sapto Wibowo & Muhamad Rifa 2015, 'Maximum Power Point Tracking for Photovoltaic using Incremental Conductance Method', Energy Procedia, vol.68, pp.22-30.

[43] Rezk, H, Aly, M, Al-Dhaifallah, M & Shoyama, M 2019, 'Design and Hardware Implementation of New Adaptive Fuzzy Logic-Based MPPT Control Method for Photovoltaic Applications', IEEE Access, vol.7, pp.106427-106438.

[44] Rokeya Jahan Mukti & Ariful Islam 2015, 'Modeling and performance analysis of PV module with Maximum Power Point Tracking in Matlab/Simulink', Applied Solar Energy, vol.51, no.4, pp.245–252.

[45] Rozana Alik & Awang Jusoh 2017, 'Modified Perturb and Observe (P&O) with checking algorithm under various solar irradiation', Solar Energy, vol.148, pp.128-139.

[46] Saban Ozdemir, Necmi Altin & Ibrahim Sefa 2017, 'Fuzzy logic based MPPT controller for high conversion ratio quadratic boost converter', International Journal of Hydrogen Energy, vol.42, no.28, pp. 17748-17759.

[47] Sabir Messalti, Abdelghani Harrag & Abdelhamid Loukriz 2017, 'A new variable step size neural networks MPPT controller: Review, simulation and hardware implementation', Renewable and Sustainable Energy Reviews, vol.68, no.1, pp. 221-233.

[48] Sakh Mozaffari Niapour, S, Danyali, MBB, Sharifian, MR & Feyzi 2011, 'Brushless DC motor drives supplied by PV power system based on Z-source inverter and FL-IC MPPT controller', Energy Conversion and Management, vol.52, no.8–9, pp. 3043-3059.

[49] Samani, L & Mirzaei, R 2019, 'Model predictive control method to achieve maximum power point tracking without additional sensors in stand-alone renewable energy systems', Optik, vol. 185, pp.1189-1204.

[50] Solangi, KH, Islam, MR, Saidur, R, Rahim, NA & Fayaz, H 2011, 'A review on global solar energy policy, Renewable and Sustainable Energy Reviews', vol.15, no. 4, pp. 2149-2163.

[51] Zainal, NA, Yusoff, AR & Apen, A 2019, 'Integrated cooling systems and maximum power point tracking of fuzzy logic controller for improving photovoltaic performances', Measurement, vol.131, pp.100-108.

[52] Zou, Y, Yan, F, Wang, X & Zhang, J 2019, 'An Efficient Fuzzy Logic Control Algorithm for Photovoltaic Maximum Power Point Tracking under Partial Shading Condition', Journal of the Franklin Institute, vol. 357, no. 6, pp. 3135-3149.